*Bulletin de l'Institut Scientifique, Rabat, Section Sciences de la Terre, 2024, n° 46, 31–53* **e-ISSN : 2458-7184**

# Geochemical feature of the Mangodara metavolcanic rocks within the Banfora Paleoproterozoic greenstone belts, southern Burkina Faso (West African Craton)

## *Caractéristiques géochimiques de métaformations volcaniques de la ceinture Paléoprotérozoique de Banfora, Sud du Burkina Faso (Craton Ouest Africain)*

**Bernadin Gnamou[1], Hermann Ilboudo[1]*, Wilfried Antoine Bassou Toe[1], Sâga Sawadogo[1]**

1. *Université Joseph KI-ZERBO. UFR/SVT. Département des Sciences de la Terre, Laboratoire Géosciences et Environnement, 03 BP 7021 Ouagadougou 03, Burkina Faso. bernadingnamou1610@gmail.com*

**Abstract.** We present new geochemical data on the volcanic rocks of the Mangodara sector (southeastern edge of the Banfora Paleoproterozoic belt) in the West African Craton and discuss their petrology and geodynamic context. Three main volcanic units are described, notably andesites, dacites, and rhyolites. These lithologies are dominated by volcanoclastite units, indicative of high-volatile explosive eruption products in the Mangodara sector. Andesite, with ΣREE=105.95 to 135.95 ppm, show LREE enrichment compared to HREE and $(La/Yb)_N$ = 6.19 - 8.25, $(La/Sm)_N$ = 3.32 - 3.95. All profiles show a Eu negative anomaly with a Eu/Eu* ratio = 0.72 - 0.94. Dacite, with ΣREE = 115.09 ppm to 118.75 ppm, shows LREE enrichment compared to HREE $(La/Yb)_N$= 6.64 - 12.42, $(La/Sm)_N$ = 3.48 - 3.67, and Eu negative anomaly with Eu/Eu* = 0.77 - 0.83. Rhyolite, with ΣREE =110.93 to 142.18 ppm shows LREE enrichment compared to HREE $(La/Yb)_N$ = 6.65 - 13.95, $(La/Sm)_N$ = 3.37 - 3.68 and Eu/Eu* = 0.78 - 0.83. Dacite, felsic volcanoclastite (rhyolite) and andesite REE patterns are parallel, suggesting a cogenetic source. Negative Nb, Ta, Ti and Sr anomalies and the lack of garnet signature in andesite, dacite and felsic volcanoclastite (rhyolite) characterize partial melting to amphibolite facies. However, the rhyolite flow shows a garnet signature. The negative Nb, Ta and Sr anomalies, the positive Pb anomaly and the low Cr and Ni content indicate melting of the middle continental crust at the start of subduction. Volcanic rocks show generally positive correlations in the La versus $(La/Sm)_N$ diagram, indicating that they may originate from different degrees of partial melting of the same crustal source. The hypothetical scenario for the origin of the Banfora belt corresponds to an individual, isolated volcanic arc.

**Keywords:** Volcanism, Subduction, Geodynamic, Paleoproterzozoic, West Africa Craton, Banfora Belt, Mangodara.

**Résumé.** Nous présentons les nouvelles données géochimiques des unités volcaniques du secteur de Mangodara au sud du Burkina Faso dans la ceinture Paléoprotérozoïque de Banfora au sein du Craton Ouest Africain. Nous discutons du mode d'association des assemblages lithologiques et du contexte géodynamique de mise en place. Trois unités sont décrites à savoir les andésites, les dacites et des rhyolites. Ces roches sont dominées par des occurrences volcanoclastiques indicatrices d'éruption de magma de forte volatilité dans le secteur. Les andésites, avec ΣREE=105,95 - 135,95 ppm, montrent un enrichissement en LREE comparé au HREE et des rapports $(La/Yb)_N$ = 6,19 - 8,25, $(La/Sm)_N$ = 3,32 - 3,95. Tous les profiles présentent une anomalie négative en Eu avec Eu/Eu* ratio = 0,72 - 0,94. Les dacites, avec ΣREE = 115,09 - 118,75 ppm présentent un enrichissement en LREE comparé à HREE. De plus, elles montrent des rapports $(La/Yb)_N$ = 6,64 - 12,42, $(La/Sm)_N$ = 3,48 - 3,67 et une anomalie négative en Eu (Eu/Eu* = 0,77 - 0,83). Les rhyolites, avec ΣREE =110,93 to 142,18 ppm présentent un enrichissement en LREE comparé au HREE et des rapports $(La/Yb)_N$ = 6,65 - 13,95, (La/Sm)N = 3,37 - 3,68 et Eu/Eu* = 0.78 - 0,83. Les dacites, les volcanoclastites (rhyolite) et les andésites présentent un profil de REE parallèle, plaidant pour un lien cogénétique. Les anomalies négatives en Nb, Ta, Ti et Sr et l'absence d'une signature de grenat dans ces unités est caractéristique d'une fusion partielle au faciès amphibolite. Cependant, les coulées rhyolitiques montrent une signature en grenat. Les anomales négatives en Nb, Ta et Sr, l'anomalie positive en Pb couplée au faibles valeurs enregistrées en Cr et Ni suggèrent une fusion de la croûte continentale moyenne en début de subduction. Les roches volcaniques montrent des corrélations généralement positives dans le diagramme La versus $(La/Sm)_N$, indiquant qu'ils peuvent provenir de différents degrés de fusion partielle de la même source crustale. Par conséquent, le scénario hypothétiques pour l'origine de la ceinture de Banfora correspond à un arc volcanique individuelles et isolées.

**Mots clés** : Volcanisme, Subduction, Géodynamique, Paléoprotérozoïque, Craton Ouest Africain, Ceinture de Banfora, Mangodara

## INTRODUCTION

The chemical composition of derived mantle reflects not only their source, but also the intensity of mixing between the various source components, the degree of melting and/or fractional crystallization, in addition to crustal contamination and tectonic settings (Niu & O'Hara 2003, Münker *et al.* 2003, Condie 2005, Arevalo & McDonough 2010, Palme *et al.* 2014, Pearce *et al.* 2021). Furthermore, any geodynamic reconstruction takes into account fundamental geochemical characteristics, including their geochemistry, nature and conditions of partial melting of sources (La flèche *et al.* 1998, Münker *et al.* 2003, Niu & O'Hara 2003, Condie 1994, 2014, Mo *et al.* 2008, Pearce 2008, Nui *et al.* 2009, Babechuk & Kamber 2011, Pearce *et al.* 2021). The Paleoproterozoic Birimian greenstone belts are characterized by lithostratigraphic succession comprising a lower major tholeiitic basaltic suite (pillow basalts) with some intercalations of sedimentary rocks, overlain by detrital and chemical sedimentary rocks (shales, sandstones, volcaniclastic and carbonate rocks) in association with calc-alkaline plutonovolcanic rocks (Bassot 1987, Abouchami *et al.* 1990, Leube *et al.* 1990, Sylvester & Attoh 1992, Feybesse & Milési 1994, Bossière *et al.* 1996, Hirdes *et al.* 1996, Pouclet *et al.* 1996, 2006, Lompo 2009, Baratoux *et al.* 2011,

Ilboudo *et al.* 2020, 2021, Mériaud *et al.* 2020, Hayman *et al.* 2023). Several tectonic models related to subduction and arc setting (Baratoux *et al.* 2011, Block *et al.* 2016, Petersson *et al.* 2016, Eglinger *et al.* 2017, Parra-Avila *et al.* 2017, 2018, 2019, Ilboudo *et al.* 2021) and mantle plumes (Lompo 2009, Vidal *et al.* 2009, Ganne *et al*. 2014, Augustin *et al.* 2017, Bonzi *et al.*2021) have been proposed for the evolution of Paleoproterozoic formations. Geochemical studies of these birimian rocks show that volcanic activity (lavas and pyroclastic rocks) has a calc-alkaline to tholeiitic affinity, suggesting bimodal volcanism (Baratoux *et al.* 2011, Ilboudo *et al.* 2020, Mériaud *et al.* 2020, Ilboudo *et al.* 2021, Hayman *et al.* 2023). Based on geochemical data from granitic rocks in the Baoulé Mossi domain, Parra -Avila *et al.* (2019) showed that magmatism evolved from east to west and from the oldest (> about 2100 Ma) to the youngest (< 2100 Ma). The present study deals with geochemical data from volcanic rocks exposed in south of the Banfora belt, in the northern extension of Côte d'Ivoire. The belt is fairly documented in the literature compared to both the Houndé and the Boromo belts in terms of their geochemical characteristics (Baratoux *et al.* 2011, 2015, Metelka *et al.* 2011, Hein *et al.* 2015, Ouiya *et al.* 2016, 2020, 2022, Augustin & Gaboury 2017, 2019, Ilboudo *et al.* 2017, 2020, Parra-Avila *et al.* 2019). However, Baratoux *et al*. (2011) and Metelka *et al*. (2011) have highlighted a possible link between the three belts since they describe similar volcanic units, in particular the eastern edge of this belt and the western margin of the Houndé belt. According to Parra-Avila *et al.* (2019), the Banfora belt has a εHf signature that indicates strong crustal reworking and contamination; thus it is considered as the boundary between the eastern and western block of the Baoulé Mossi domain. The volcanic activity that prevailed in western Burkina Faso took place between 2190 Ma and 2160 Ma (Eoeburnean) according to Baratoux *et al.* (2011) but that of the Banfora belt shows a juvenile character with regard to εHf values (~ 0 to + 8) according to Parra-Avila *et al*. (2019). Geochemically, the associated granitic intrusions have an arc-like character, including negative Ta, Nb and Sr anomalies and a predominantly older than 2100 Ma (Parra -Avila *et al.* 2019) and evolves from east to west (Ilboudo *et al.* 2020). The geochemical signature of Banfora belt rocks shows different geodynamic settings evolving from komatiite to calc-alkaline affinity (Ilboudo *et al.* 2020). Despite the overall body of work, a better understanding of geology is necessary, particularly in the Mangodara sector that present metallogenic interest. In this study, we will discuss the geochemical characteristics of volcanic unit in this part of the Birimian system, not yet investigated.

## GEOLOGICAL SETTING

Several studies (Kouamelan 1996, Caby & Agoh., 2000, Castaing *et al.* 2003, Rollinson 2016, Block *et al.* 2016, Markwitz *et al.* 2016) present the geological configuration of the Léo/Man shield in two domains, respectively the western Kénéma-Man domain > 2,500 Ma and the eastern Baoulé-Mossi domain dated at ~2000 Ma (Kouamelan 1996, Parra-Avila *et al*. 2017). The Baoulé-Mossi domain consists mainly of volcanic and sedimentary belts andgranitoid

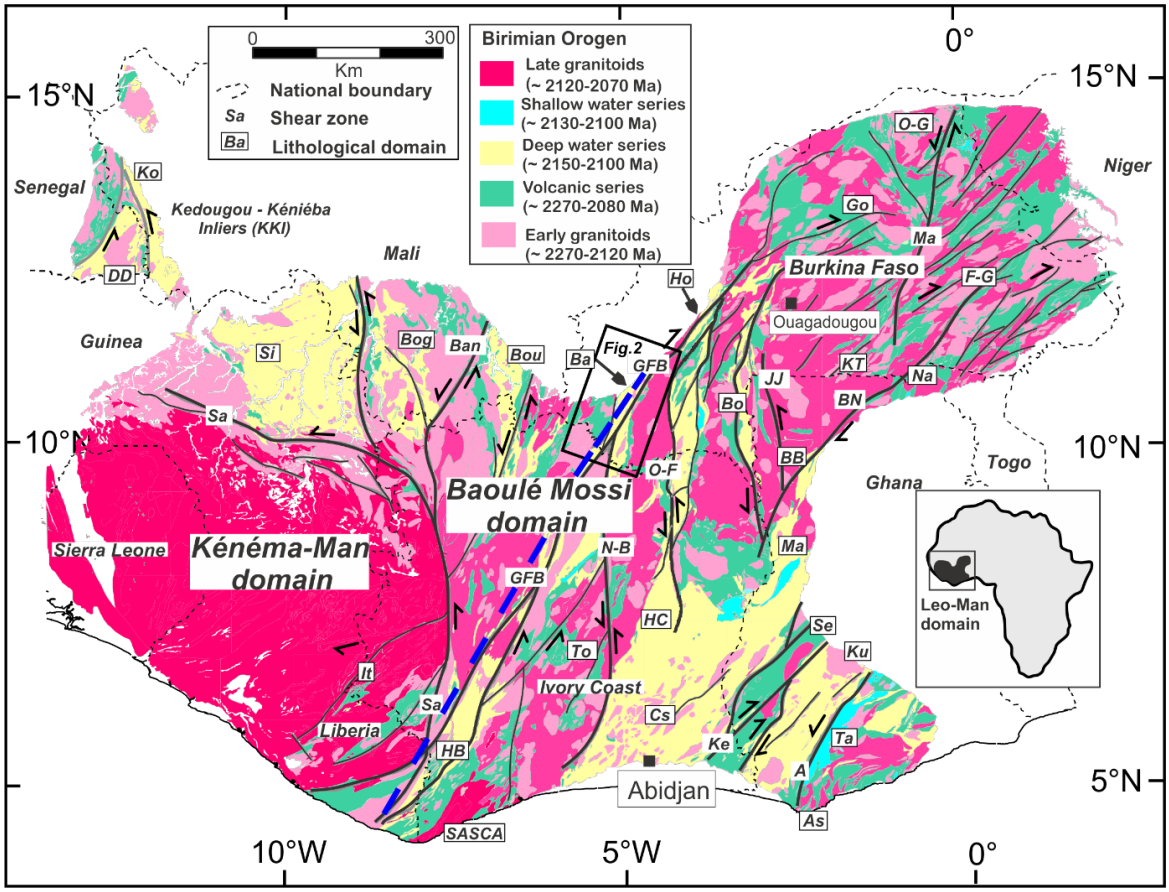


Figure 1: (a) geological map of the Leo/Man shield and the most important gold deposits across the WAC (modified from Grenholm et al. 2019). As: Ashanti series; Ta: Tarkwaian series; Ku: Kumasi series; Se: Sefwi series; CS – Comoé-Sunyani series; Ma – Maluwe series; Na – Nangodi series; BB – Bolé-Bulenga domain; La – Lawra series; Bo: Boromo series; KT: Kedougou-Tumu domain; Go: Goren series; OG: Oudalan-Gouroul domain; OF – Ouango-Fitini Shear zone; HC – Haute Comoé series; HB – Hana Lobo–Bandama; Ba: Banfora series; It: Ity-Toulepleu inlier; BB: Boundiali–Bagoé; Bo: Bogouni; Si – Siguiri series; Ko: Kofi series; DD: Dialé-Daléma series; Ma: Mako series.

intrusions (Castaing *et al.* 2003, Lompo 2009, 2010, Vidal *et al.* 2009, Baratoux *et al.* 2011, Ganne *et al.* 2014, Block *et al.* 2016, Augustin *et al.* 2017, Parra-Avila *et al.* 2019, Grenholm *et al.* 2019, Bonzi *et al.,* 2021, 2022). Burkina Faso which extends onthe Baoulé-Mossi domain is composed of a Paleoproterozoic basement greenstone andgranitoid belts (80%) covered in its western, northern and eastern margin by Neoproterozoicto Cambro-Ordovician sedimentary (1000 - 435 Ma) formations (20%). The belts are essentially made up of metavolcanic rocks, ranging from metabasalts to metarhyolites and metasedimentary rocks including quartzites and metapelites (Milési *et al.* 1989, Baratoux *et al.* 2011, Ilboudo *et al.*2017, 2020). Specifically, the Banfora belt that extends over several kilometers in Burkina Faso lays up to Côte d'Ivoire; and is intersectedby the Bobo-Dioulasso high strain corridorrepresenting the continuity of the majorGreenville-Ferkéssédougou-Bobo-Dioulasso shear zone (Fig. 1).

The eastern part of the Banfora belt consists of interlayered units of basalts, andesites, volcano-sediments and rhyolites (Fig. 2), 2 to 4 km thick, while the western part is composed solely of volcano-sediments according to Baratoux *et al.* (2011).The global stratigraphy ofthe belt proposed by these authors and revised by Ilboudo *et al.* (2020) suggests, from bottom to top (Fig. 3): (i) deposition of ultramafic rock, (ii) deposition of mafic volcanics, (iii) subsequent deposition of lava flow and projection (pyroclastite and lapilli tuff), (iv) depositionof siliceous rock (exhalite), (v) emplacement of pelitic and turbiditic sediments, (vi) emplacement of the pre-collision eastern granite and (vii) emplacement of the post-collision western granite. The volcanic activity that prevailed in West Burkina Faso took place between 2190 Ma and 2160 Ma (Eoeburnean) according to Baratoux *et al.* (2011) and presents a juvenile character with regard to εHf (~ 0 to + 4) (Parra-Avila *et al.* 2019). The exhalites constitute theupper horizon of the lithostratigraphy of the volcanic formations of the eastern part of the beltand subvolcanic rocks consist mainly of porphyry microdiorite, dolerite sillsand dykes (Ilboudo *et al.* 2020). Syn-tectonic intrusions (granite and granodiorite) emplaced in the favor of Greenville-Ferkéssédougou-Bobo-Dioulasso regional shear zone known from Liberia and Côte d'Ivoire (Ouattara1998, Baratoux *et al.* 2011, Ilboudo *et al.* 2020). Based on geochemical and geotectonic setting, Ilboudo *et al.* (2020) pointed out that granitoids in western and eastern margins of theBanfora belt are

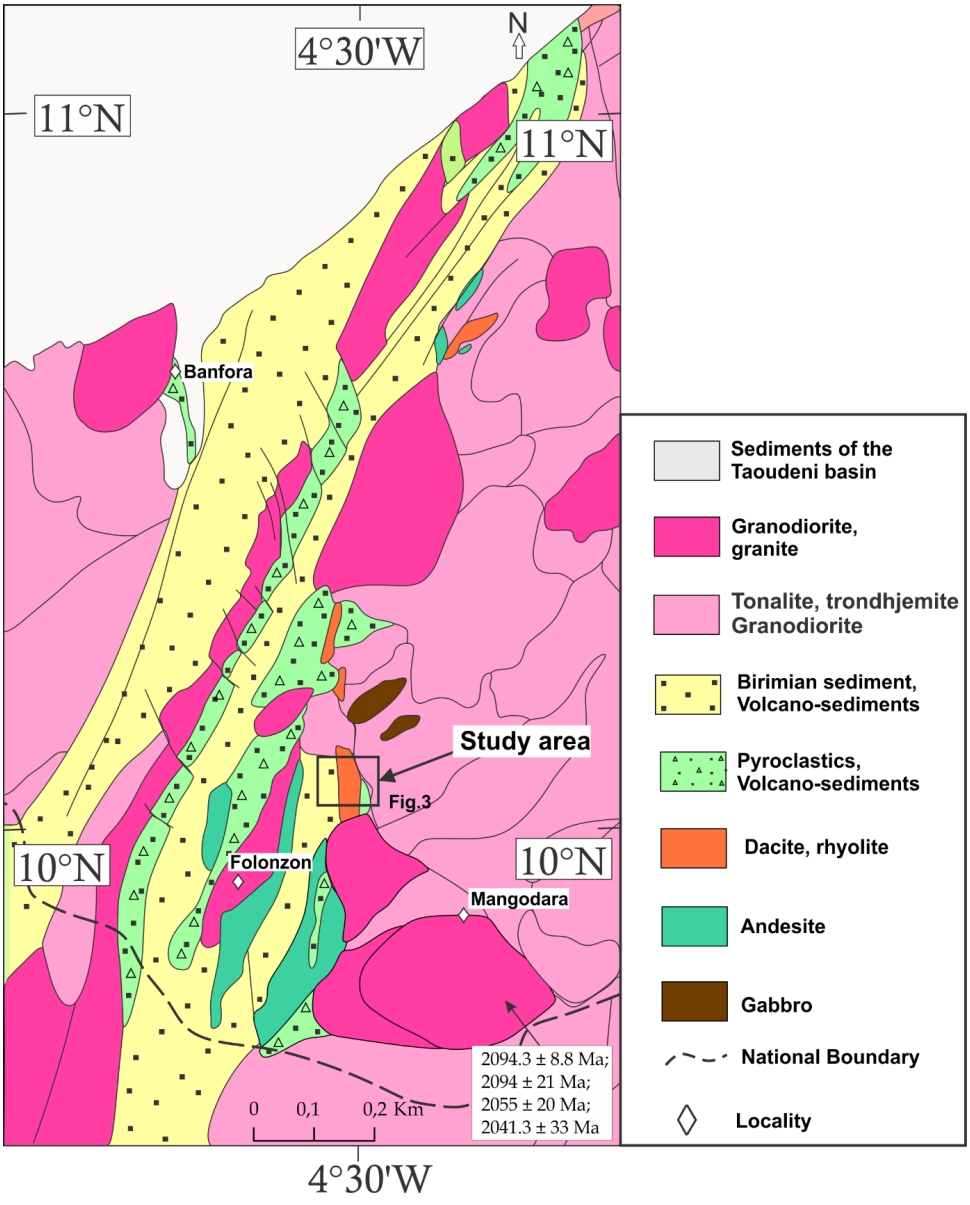


Figure 2: simplified geological map of Banfora green belt (modified from Metelka et al., 2011) and location of the studied area.

respectively post-and pre-collisional. Geochemically, granitoid intrusions show arc volcanic incharacter, including negative Ta, Nb and Sr anomalies and mostly older than 2100 Ma (Parra-Avila *et al.* 2019). In nearby area, pegmatite associated to granitoids and migmatitic gneisspotentially contains rare metals (Bonzi *et al.* 2021, 2022).

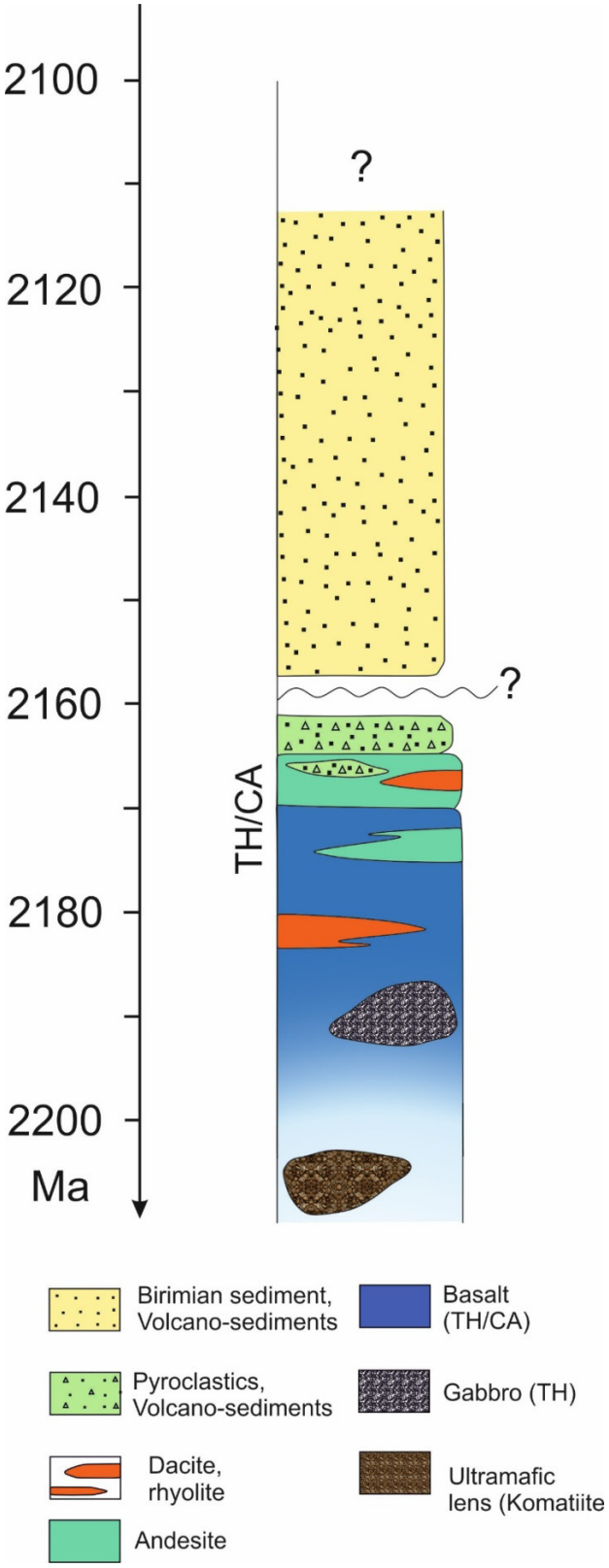


Figure 3: Simplified stratigraphic sequences for the Banfora (modified from Baratoux *et al*., 2011)

The study area consists of a set of dominantly metamorphosed volcanic formations (rhyolite, rhyolitic tuff, dacite, andesite, basalt (Fig. 4a and b). Rare outcrops of sulphidic felsic and highly siliceous formations (rhyolite, cherts and quartzites) that have resisted to the weathering appear as main host rocks (Ilboudo *et al.* 2017). Late monzonite, granodiorite and diorite cross cut the entire volcanicpackage.

## METHODOLOGY

### Sampling

The fieldwork consisted of describing and sampling several diamond drillholes for further investigations. The samples come from two drillholes (K7 and K15), following a good spatial coverage of the alteration zones. A total of fifty rock samples from these drillholes were collected. The sampling was undertaken on the different lithologies. Fifty thin sections were made, including twenty at Western Australia University and thirty at Université Joseph KI-ZERBO at the Laboratoire Geosciences et Environment (LaGE). Detail investigation is operated under a Nicon Eclipse 50i POL type polarizing microscope (transmitted and reflected lights), coupled to a camera.

### Analytical method

Part of this study is based on whole-rock geochemical data from the drill cores. Samples were analyzed by XRF diffraction for major, rare earth and trace elements by Inductively Coupled Plasma Mass Spectrometry (ICP-MS) at the ACME Laboratory in Vancouver. Twenty-one of the analyzed samples were from andesite, dacite and rhyolite (Tab. 1). Samples were crushed and pulverized to 200 mesh and sample fragments (0.2 g) were placed in graphite crucibles and with lithium borate flux added. The crucibles were placed in an oven and heated at 1025°C for 25 min. Each melted sample was then dissolved in 5% HNO3. A blank and internal standard (STD SO-15 reference material) were carried through the weighing, digestion, and analysis stages to check for accuracy. Calibration standards, verification standards, and reagent blanks were also added to the sample sequence for testing.

## RESULTS

### Lithology

#### *Meta-andesite*

The meta-andesite unit comprises coherent andesite and volcanoclastite. The contact of coherent andesites with other lithologies is clear, although contacts are frequently overprinted by pervasive alteration. The matrix is generally grayish in the absence of intense hydrothermal alteration (Fig. 5a), whereas altered andesites show different colors, (i) dark green from chlorite alteration and (ii) greenish-gray to beige with intense silky sheen from sericite-chlorite alteration.

The meta-andesite flow is characterized by a microlithic and porphyritic texture (Fig. 5b). Phenocrystals are plagioclase (10-15 vol.%) (1-2 mm) and biotite (15-25 vol.%) (1-1.5 mm) and the matrix contains common mineral assemblage such as plagioclase (20 - 25 vol.%), hornblende (1 - 20 vol.%), biotite (15 - 35 vol.%) (Fig. 5c and d). Associated alteration mineral varies depending on the degree of alteration and are resumed to carbonate (2 - 10 vol.%), sericite (5 - 20 vol.%), epidote (1 - 2 vol.%), chlorite (10 - 20 vol.%). Commonly opaque minerals (pyrite and pyrrhotite) are found. Biotite, in clusters of flakes, develops brown to black screens, either as a sheet

associated with carbonate veins, or as aggregates in a matrix of sub-grained recrystallized quartz. Plagioclase phenocrysts turn into sericite, albite or carbonate.

Volcaniclastic occurrences are the most abundant unit (Fig. 6a). They consist locally of a monomictic breccia supported by angular clasts in a carbonate-rich matrix typical of hydrothermal brecciation (Fig. 6b). The mineral assemblage associates secondary quartz (10-30 vol. %), plagioclase (20 – 25 vol. %), biotite (15 – 20 vol. %), hornblende (2-5 vol. %), chlorite (2 – 5 vol. %), carbonate 0 – 20 vol. % (Fig. 6c and d). Opaque minerals are, pyrite (5 – 15 vol. %), pyrrhotite (3 - 15 vol. %), chalcopyrite (0 - 5 vol. %). Secondary quartz is often associated with sulphide veinlets. Biotite coexists with hornblende (Fig. 6d). Carbonate, chlorite, sericite or secondary quartz and epidote develops groundmass that represents the pervasive alteration.

### *Metadacite*

Compared to meta-andesite, metadacities outcrop as massive homogenous facies, but they are mesocratic and microlitic (Fig. 6e), although frequently overprinted by pervasive sericite alteration. This unit is commonly spatially associated with andesite. Minerals consist of quartz and plagioclase phenocrysts (Fig. 6f), overall reaches 1 vol.% within fine and microcrystalline matrix made up of quartz (10-15 vol.%) quartz, plagioclase (10-20 vol.%) deformed and altered into sericite while biotite (10-20 vol.%) breaks to chlorite. Albite phenocrysts (< 1%, 0.5 to 1 mm) are weakly stretched and altered.

### *Metarhyolite*

Metarhyolites are the most abundant volcanic rocks in the study area, among which we describe two types, namely the dominated highly altered metarhyolite tuff and minor felsic volcaniclastic

The metarhyolite tuff exhibits a diversity of textural appearance, ranging from light gray to beige and an intense silky sheen from sericite alteration; light blue to bluish and silky sheen from sericite-chlorite alteration (Fig. 7a); grayish due to abundant kyanite (Fig. 7b) and beige-gray to white from sericite-silica alteration. Those appearances are associated to aphanitic and locally porphyroblastic texture made up of blue quartz (0.5 - 1 mm, 5 - 10 vol.%), kyanite (1 - 2 mm, 0 - 50 vol.%), staurolite (1 - 2 mm, 0 - vol. 30%) and garnet (1 - 3 mm, 0 - 10 vol.%) overprinted by a lepidoblastic texture (Fig. 7c). The matrix (70 vol.%) consists of corroded quartz grain associated with sub-grained recrystallized quartz (30 - 40 vol.%), sericite flakes 20 - 30 vol.% (Fig. 7d) and chlorite (0 - 10 vol.%). Brecciated occurrences consist of a monomictic breccia supported by felsic clasts, showing angular and puzzle-shaped blocky textures within chlorite and/or tourmaline matrix.

The felsic volcanoclastite is leucocratic and aphanitic (Fig. 7e), although it is frequently overprinted with tourmaline veinlets and penetrative schistosity. The unit consists of hydrothermal breccia showing a blocky, puzzle-like texture in a tourmaline-rich matrix. The mineralogical composition combines primary (5 – 10 vol.%) and secondary (30 - 40 vol.%) quartz, plagioclase (1-5 vol.%), tourmaline (5-10

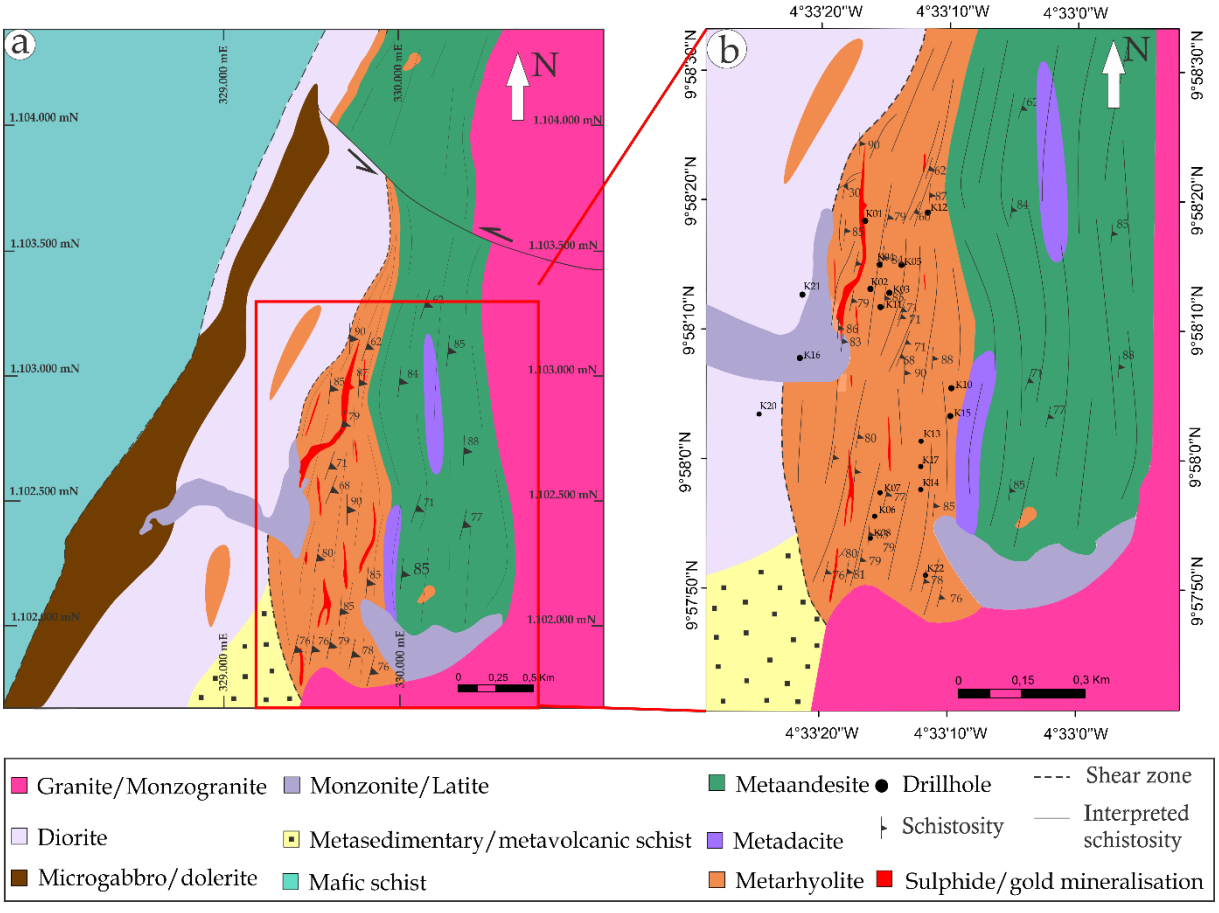


Figure 4: Geology environment. (a): regional geology; (b); geological map of the study area.

vol.%), biotite (1-2 vol.%). Alteration mineral are chlorite (2-3 vol.%), sericite (5-10 vol.%), carbonate (5-15 vol.%). It consists of 5 - 8 vol.% corrode or poikilitic quartz with sub-grain recrystallization at the edges (Fig. 4f) and rare plagioclase crystals (1 %) in the matrix. Tourmaline represents around 30 vol.% of the products of hydrothermal alteration, and occurs as crystals (Fig. 7f) and veinlets in the matrix.

## Geochemical data

### *Lithogeochemistry*

Mangodara volcanic rocks were classified using two diagrams: Nb/Y vs. Zr/Ti (Pearce 1996) and $Zr/TiO_2$ vs. $SiO_2$ (Winchester & Floyd 1977). The samples fall within the rhyolite/dacite and andesite/basaltic andesite field (Fig. 8a) in the Nb/Y vs. Zr/Ti diagram. The rhyolite and dacite samples lie in the rhyodacite/dacite field, except one sample in the rhyolite field and the andesite samples in the andesite field in the $Zr/TiO_2$ vs. $SiO_2$ diagram (Fig. 8b). This shows that the rhyolites in the Mangodara area are enriched in titanium oxide ($TiO_2$).

### *Trace element data analysis*

The composition of incompatible (La, Rb, Zr, Ba, Th, Nd) and compatible (Sr, Ni, Cr, V, Y, Yb) trace elements (Tab. 1) vary considerably in the three volcanic units. Rb (40.93- 77.86 ppm), Ba (561.70 - 927.29 ppm), Sr (97.76 - 258.17 ppm), Zr (102.09 - 142.19 ppm), Nb (4.53 - 9.89 ppm), Ta (0.46 - 0.85 ppm) confirm this variability in andesite. Similarly, dacite shows slightly variable contents of Rb (57.61 - 86.79 ppm), Ba (526.79 - 687.29 ppm), Sr (105.98 - 258.17 ppm), Zr (114.19 - 114.90 ppm), Nb (2.58 - 2.69 ppm), Ta (0.33- 0.34 ppm). Compared to andesite, Rb (17.43 - 90.23 ppm), Ba (301.79 - 1907ppm), Sr (122.70- 171.07 ppm), Zr (124.09 - 199.5 ppm), Nb (1.48- 2.82 ppm), Ta (0.15 - 0.30 ppm) are more variable in rhyolite. All volcanics have La/Nb, Th/Nb, Th/La, Th /Yb, La/Yb ratios lower than the lower continental crust (Tab. 2, Rudnick & Gao, 2014). To better define the magmatic affinities of the lithologies, we used modern immobile element affinity diagrams elaborated according to Co vs Th (Hastie *et al.* 2007). The diagram shows that andesites, dacites, and rhyolites, have a calc-alkaline affinity (Fig. 9).

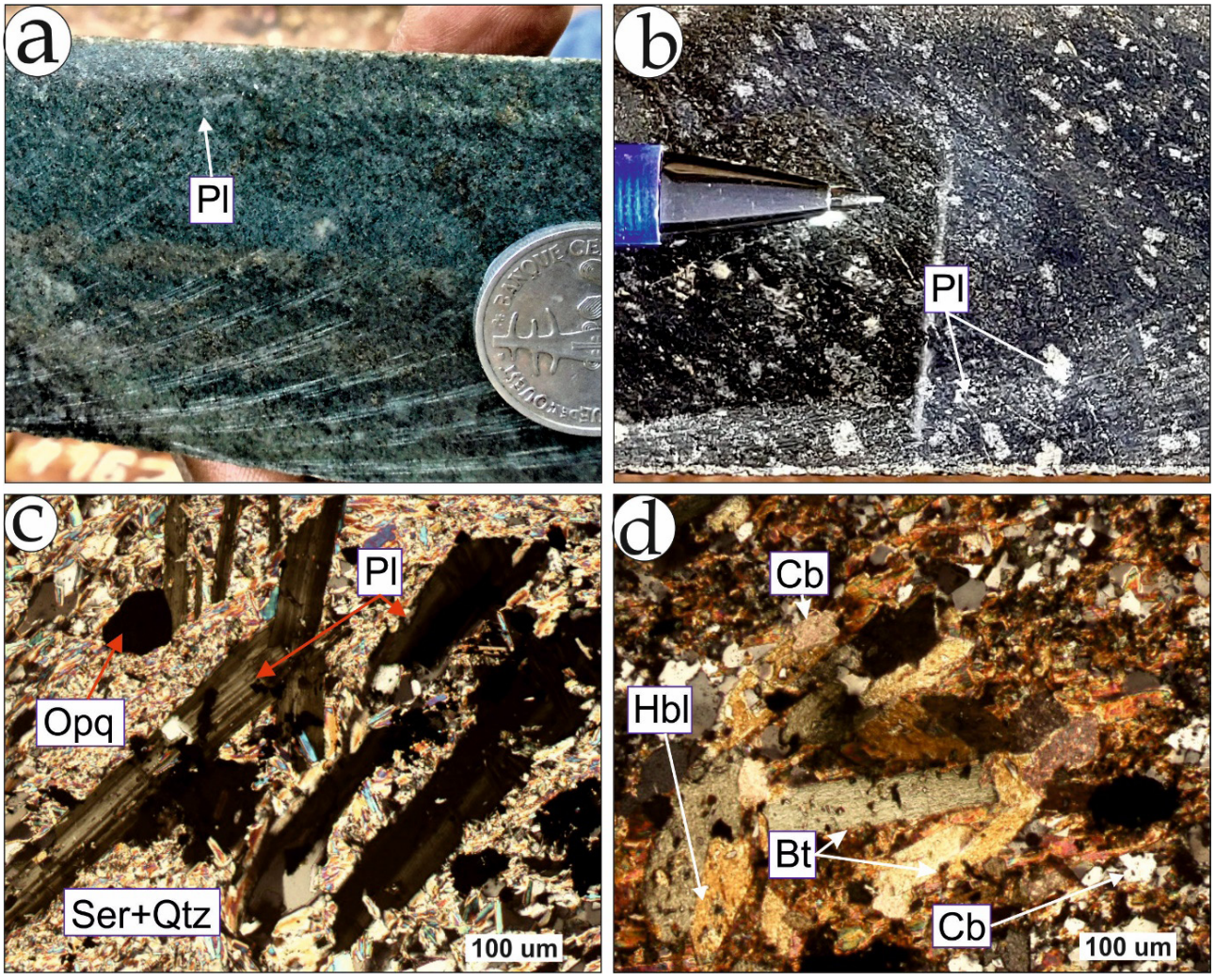


Figure 5: (a) dark green from chlorite alteration in andesite; (b): plagioclase phenocrystal in andesite; (c): plagioclase phenocrysts in a sericite - quartz matrix in andesite; (d): honblende and carbonate associated with biotite clusters. Pl : Plagioclase; Chl : Chlorite; Qtz : Quartz ; Bt : Biotite ; Hbl : Hornblende ; Opq : Opaque ; Chl : Chlorite ; Cb : Carbonate.

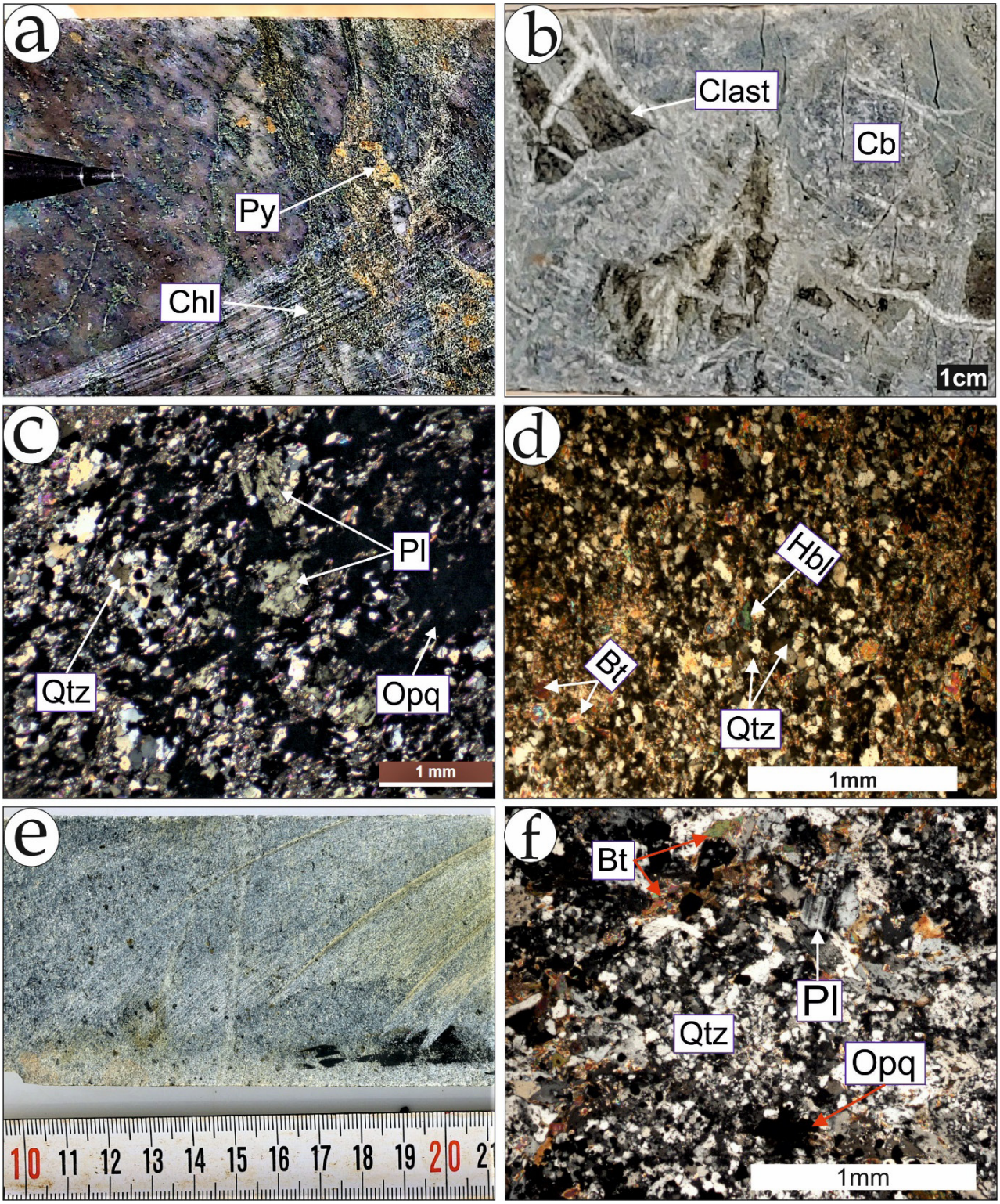


Figure 6: Samples from drill core and microphotograph of the main lithologies. (a): Intermediate volcanoclastite; (b): Intermediate volcanoclastite brecciated by hydrothermal fluid; (c): microphotograph of the Intermediate volcanoclastite composed of plagioclase and secondary quartz; (d): microphotograph of the Intermediate volcanoclastite composed of hornblende, biotite and secondary quartz; (e) Macrophotograph of metadacite; (f) microphotograph of the metadacite composed of plagioclase, biotite and quartz. Pl : Plagioclase ; Ser : Séricite ; Qtz : Quartz ; Bt : Biotite ; Hbl : Hornblende ; Opq : Opaque ; Chl : Chlorite ; Cb : Carbonate.

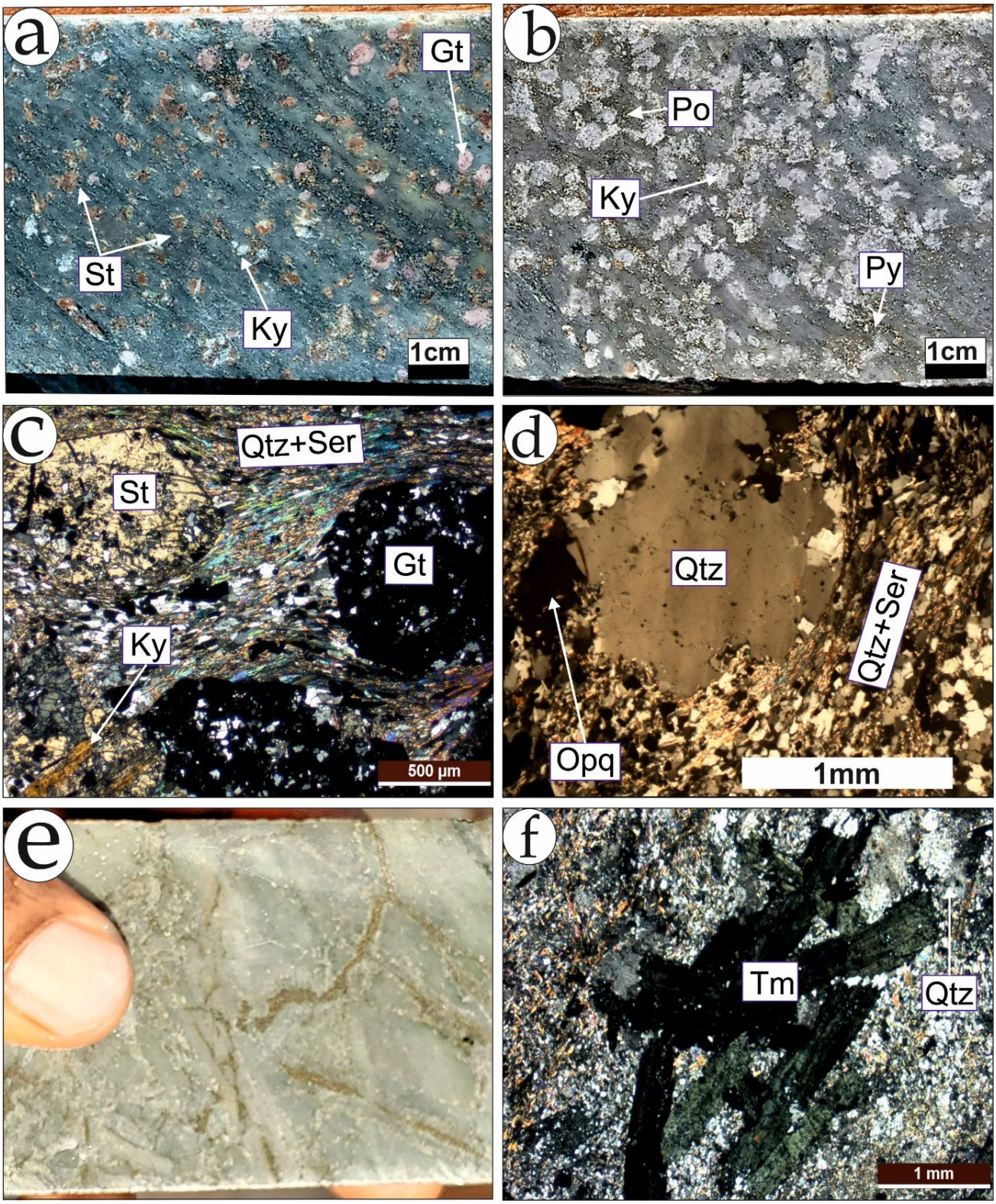


Figure 7: Samples from drill core and microphotograph of the main lithologies. (a) kyanite – staurolite -garnet porphyroblast in metarhyolite tuff; (b): kyanite porphyroblast in metarhyolite tuff; (c): microphotograph kyanite – staurolite -garnet porphyroblast in metarhyolite tuff; (d): primary corroded quartz in a sericite - quartz matrix in metarhyolite tuff; (e) Macrophotograph of felsic volcanoclastite; (f) Tourmaline porphyroblast in felsic volcanoclastite. Pl : Plagioclase ; St: Staurotide ; Ky: Kyanite ; Qtz : Quartz ; Gt : Garnet ; Py : Pyrite ; Po : Pyrrhotite ; Tm: Tourmaline; ; Ser : Séricite; Opq: Opaque.

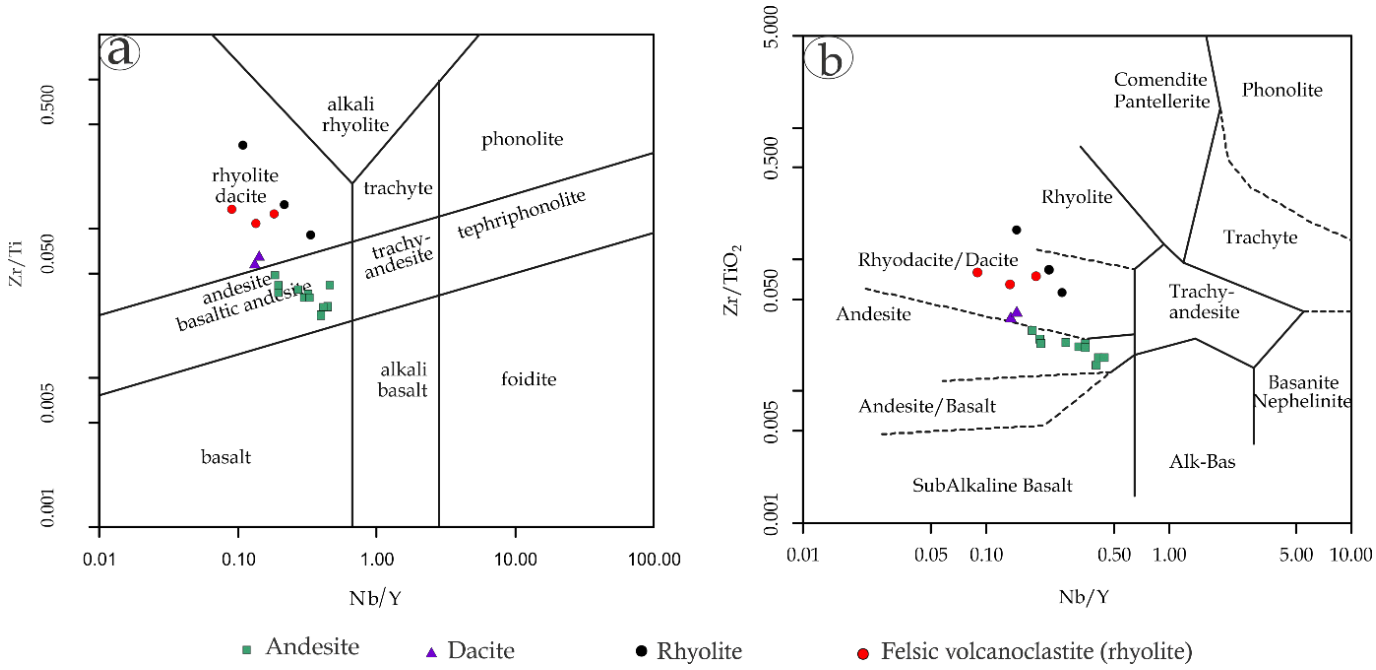


Figure 8: Diagram of classification of different volcanic rocks. (a) : Nb/Y Vs Zr/Ti diagram (Pearce 1996); (b) : Nb/Y Vs Zr/TiO2 (Winchester & Floyd 1977).

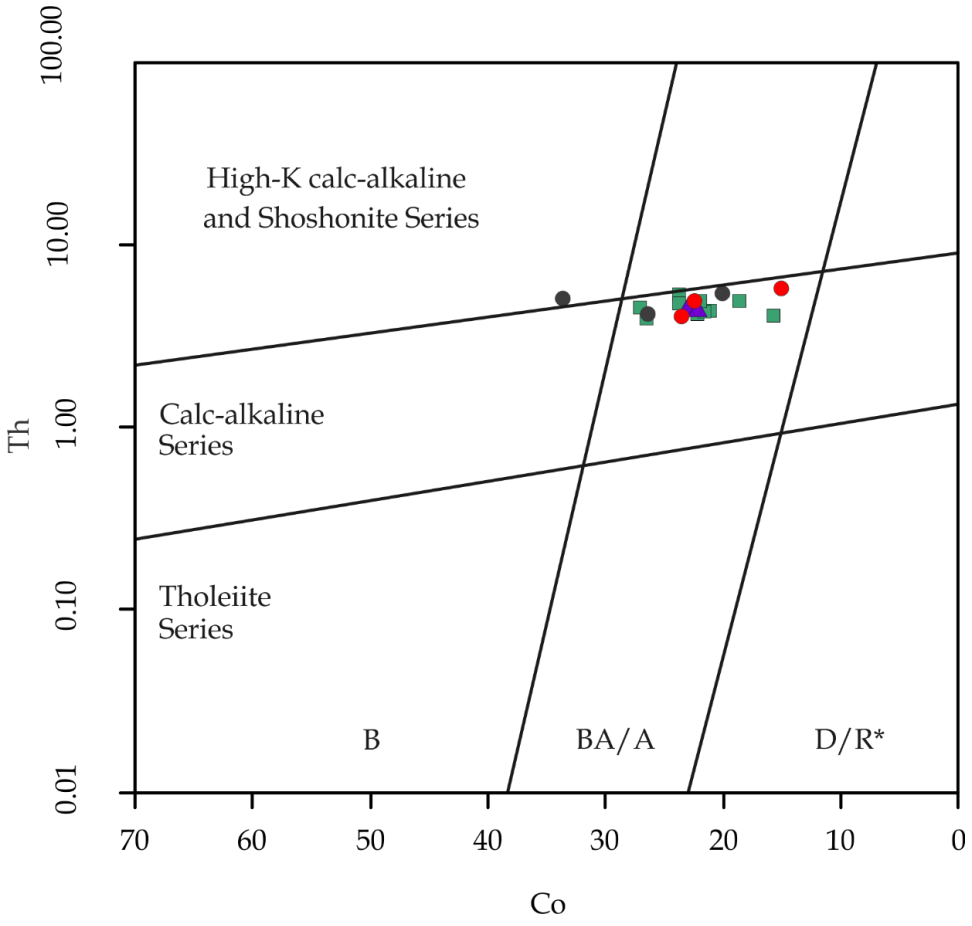


Figure 9: Hastie et al. (2007) plot of study area suite with calc-alkaline

Table 1: Lithogeochemical data of the Mangodara area.

| Sample | K7_47 | K7_163 | K7_84 | K7_151 | K15_393 | K15_187 | K15_280 | K15_323 | K7_202.86 | K7_203 | K11_33 | K11_65 | K15_85 | K15_131 | K15_257 |
|---|---|---|---|---|---|---|---|---|---|---|---|---|---|---|---|
| Element/ Oxyde | Rhyolite | Rhyolite | Rhyolite | Rhyolite | Rhyolite | Rhyolite | dacite | dacite | Andesite | Andesite | Andesite | Andesite | Andesite | Andesite | Andesite |
| SiO2 | 64.94 | 67.16 | 71.89 | 60.81 | 65.35 | 70.63 | 64.96 | 63.40 | 65.84 | 63.12 | 63.12 | 62.69 | 61.92 | 62.99 | 62.69 |
| Al2O3 | 14.70 | 15.34 | 15.37 | 7.10 | 15.10 | 8.27 | 14.40 | 14.56 | 15.25 | 15.69 | 14.22 | 14.69 | 14.23 | 13.64 | 14.15 |
| Fe2O3 | 6.72 | 7.65 | 3.96 | 11.51 | 7.58 | 6.65 | 6.31 | 7.12 | 6.05 | 7.51 | 7.31 | 7.35 | 6.78 | 6.91 | 7.64 |
| CaO | 2.62 | 0.35 | 1.17 | 0.46 | 2.62 | 0.51 | 2.09 | 4.69 | 5.65 | 6.24 | 5.07 | 5.18 | 6.08 | 5.49 | 4.40 |
| MgO | 3.23 | 0.18 | 0.31 | 0.06 | 2.40 | 0.26 | 2.42 | 3.92 | 1.45 | 1.74 | 3.82 | 4.09 | 3.47 | 3.42 | 3.31 |
| Na2O | 0.33 | 0.65 | 0.83 | 0.30 | 0.31 | 0.18 | 0.21 | 0.14 | 1.20 | 1.61 | 0.24 | 0.25 | 2.71 | 2.96 | 0.22 |
| K2O | 0.92 | 3.73 | 2.55 | 0.95 | 0.78 | 1.29 | 3.32 | 2.10 | 2.11 | 1.79 | 1.25 | 1.86 | 2.32 | 1.61 | 2.66 |
| TiO2 | 0.16 | 0.18 | 0.20 | 0.12 | 0.19 | 0.24 | 0.30 | 0.34 | 0.64 | 0.65 | 0.48 | 0.57 | 0.66 | 0.65 | 0.52 |
| P2O5 | 1.39 | 0.39 | 0.73 | 0.61 | 1.56 | 0.93 | 1.45 | 1.36 | 1.51 | 1.50 | 1.44 | 1.46 | 1.38 | 1.38 | 1.43 |
| LOI | 4.50 | 4.00 | 3.00 | 16.23 | 2.99 | 9.67 | 4.00 | 2.43 | 0.98 | 0.23 | 3.00 | 2.00 | 0.52 | 0.10 | 2.54 |
| **Total** | **99.52** | **99.64** | **100.01** | **98.16** | **98.88** | **98.64** | **99.46** | **100.06** | **100.69** | **100.08** | **99.96** | **100.14** | **100.07** | **99.14** | **99.57** |
| Au | 0.05 | 0.03 | 0.06 | 7.45 | 0.06 | 0.08 | 0.05 | 0.08 | 0.00 | 0.08 | 0.04 | 0.06 | 0.02 | 0.00 | 0.04 |
| Ag | 0.25 | 1.10 | 0.25 | 0.25 | 0.25 | 0.25 | 0.25 | 0.25 | 0.11 | 0.25 | 0.25 | 0.25 | 0.25 | 0.25 | 0.25 |
| As | 105.90 | 19.70 | 10.50 | 139.10 | 73.40 | 150.00 | 49.80 | 20.10 | 9.60 | 13.00 | 51.70 | 82.80 | 11.70 | 12.20 | 76.10 |
| Ba | 544.40 | 976.40 | 901.30 | 1907.00 | 301.80 | 411.10 | 687.30 | 526.80 | 742.80 | 697.50 | 571.20 | 658.10 | 927.30 | 721.20 | 561.70 |
| Be | 0.89 | 0.71 | 0.95 | 0.48 | 1.05 | 0.42 | 0.80 | 0.89 | 1.46 | 1.35 | 0.85 | 0.98 | 0.85 | 0.87 | 0.99 |
| Bi | 0.11 | 0.17 | 0.04 | 0.15 | 0.04 | 0.26 | 0.10 | 0.06 | 0.03 | 0.03 | 0.19 | 0.29 | 0.08 | 0.11 | 0.26 |
| Cd | 0.14 | 0.26 | 0.14 | 0.53 | 0.08 | 0.12 | 0.08 | 0.06 | 0.15 | 0.24 | 0.10 | 0.14 | 0.22 | 0.14 | 0.09 |
| Co | 22.60 | 33.60 | 14.00 | 20.90 | 23.60 | 26.00 | 23.10 | 23.00 | 18.60 | 23.70 | 22.30 | 21.90 | 21.10 | 21.70 | 22.30 |
| Cr | 100.00 | 133.00 | 83.00 | 114.00 | 85.00 | 78.00 | 81.00 | 86.00 | 91.00 | 100.00 | 88.00 | 108.00 | 73.00 | 77.00 | 82.00 |
| Cs | 1.46 | 3.12 | 2.42 | 1.52 | 1.18 | 2.53 | 3.74 | 2.88 | 6.11 | 4.46 | 3.68 | 8.14 | 4.03 | 3.38 | 4.02 |
| Cu | 44.00 | 53.00 | 31.00 | 88.00 | 95.00 | 70.00 | 45.00 | 44.00 | 45.00 | 56.00 | 75.00 | 50.00 | 47.00 | 48.00 | 58.00 |
| Ga | 16.86 | 18.34 | 16.91 | 15.59 | 16.97 | 12.53 | 16.56 | 16.42 | 17.42 | 17.68 | 16.34 | 16.22 | 16.37 | 16.03 | 16.02 |
| Ge | 0.63 | 0.91 | 1.40 | 0.28 | 0.91 | 0.37 | 0.63 | 0.85 | 1.23 | 1.08 | 0.81 | 0.76 | 0.86 | 0.81 | 0.58 |
| Hf | 3.54 | 3.85 | 3.66 | 5.16 | 3.34 | 3.58 | 3.10 | 3.02 | 2.73 | 3.04 | 2.81 | 3.18 | 3.48 | 3.35 | 3.45 |
| In | 0.03 | 0.03 | 0.03 | 0.04 | 0.03 | 0.02 | 0.04 | 0.03 | 0.05 | 0.06 | 0.05 | 0.05 | 0.05 | 0.04 | 0.03 |
| Li | 86.80 | 13.40 | 40.00 | 13.20 | 85.00 | 20.90 | 20.70 | 19.50 | 14.00 | 14.70 | 17.00 | 19.80 | 24.30 | 28.00 | 41.00 |

| Sample | K7_47 | K7_163 | K7_84 | K7_151 | K15_393 | K15_187 | K15_280 | K15_323 | K7_202.86 | K7_203 | K11_33 | K11_65 | K15_85 | K15_131 | K15_257 |
|---|---|---|---|---|---|---|---|---|---|---|---|---|---|---|---|
| Element/ Oxyde | Rhyolite | Rhyolite | Rhyolite | Rhyolite | Rhyolite | Rhyolite | dacite | dacite | Andesite | Andesite | Andesite | Andesite | Andesite | Andesite | Andesite |
| Mn | 533.00 | 46.00 | 92.00 | 54.00 | 873.00 | 168.00 | 734.00 | 874.00 | 1015.00 | 1171.00 | 986.00 | 1001.00 | 904.00 | 904.00 | 956.00 |
| Mo | 0.80 | 1.70 | 1.60 | 3.50 | 1.30 | 2.10 | 1.80 | 1.20 | 2.30 | 1.50 | 1.10 | 1.70 | 1.20 | 1.60 | 2.10 |
| Nb | 1.94 | 1.86 | 1.99 | 1.48 | 2.48 | 2.83 | 2.59 | 2.69 | 9.56 | 9.89 | 4.53 | 4.94 | 9.15 | 6.82 | 4.56 |
| Ni | 37.00 | 51.00 | 31.00 | 78.00 | 40.00 | 36.00 | 30.00 | 34.00 | 27.00 | 37.00 | 28.00 | 32.00 | 23.00 | 25.00 | 31.00 |
| Pb | 7.40 | 31.40 | 20.20 | 27.00 | 4.50 | 5.90 | 10.00 | 6.20 | 20.60 | 20.90 | 9.30 | 23.90 | 13.20 | 9.10 | 8.40 |
| Rb | 28.71 | 90.23 | 71.38 | 21.18 | 17.43 | 35.41 | 86.79 | 57.61 | 72.66 | 60.52 | 40.93 | 55.96 | 70.54 | 43.41 | 77.86 |
| S | 2.65 | 3.11 | 1.33 | 5.24 | 2.46 | 3.55 | 2.11 | 1.43 | 0.11 | 0.28 | 1.82 | 1.22 | 0.41 | 0.89 | 2.11 |
| Sb | 6.32 | 3.54 | 4.58 | 4.56 | 8.90 | 7.53 | 4.42 | 3.44 | 4.08 | 4.90 | 5.16 | 7.12 | 4.52 | 4.42 | 4.50 |
| Sc | 18.90 | 20.10 | 20.10 | 21.80 | 20.60 | 16.40 | 19.50 | 20.80 | 19.40 | 19.50 | 20.90 | 22.20 | 20.90 | 19.50 | 20.40 |
| Se | 12.70 | 0.60 | 0.70 | 3.00 | 0.60 | 6.70 | 2.00 | 0.90 | 0.25 | 0.25 | 1.70 | 0.25 | 0.60 | 1.00 | 2.60 |
| Sn | 1.40 | 1.10 | 1.30 | 0.90 | 0.60 | 0.80 | 1.50 | 1.20 | 1.90 | 2.20 | 1.50 | 1.80 | 1.90 | 1.80 | 1.20 |
| Sr | 142.78 | 122.71 | 171.07 | 144.33 | 130.20 | 145.51 | 105.98 | 149.55 | 244.67 | 258.17 | 185.77 | 183.06 | 193.42 | 182.34 | 97.77 |
| Ta | 0.30 | 0.28 | 0.28 | 0.16 | 0.30 | 0.21 | 0.33 | 0.34 | 0.72 | 0.85 | 0.51 | 0.58 | 0.61 | 0.64 | 0.47 |
| Te | 0.03 | 0.05 | 0.03 | 0.03 | 0.03 | 0.15 | 0.12 | 0.13 | 0.03 | 0.06 | 0.16 | 0.03 | 0.03 | 0.12 | 0.21 |
| Th | 4.86 | 5.11 | 5.61 | 5.85 | 4.09 | 4.32 | 4.51 | 4.44 | 4.92 | 5.42 | 4.64 | 4.94 | 4.37 | 4.35 | 4.58 |
| Tl | 0.83 | 5.18 | 1.29 | 13.63 | 0.69 | 1.70 | 1.22 | 0.81 | 0.96 | 0.75 | 0.94 | 1.07 | 0.69 | 0.50 | 1.28 |
| U | 1.44 | 1.63 | 1.78 | 2.73 | 1.40 | 1.42 | 1.51 | 1.46 | 0.71 | 0.87 | 1.54 | 1.77 | 1.47 | 1.47 | 1.57 |
| V | 116.00 | 146.00 | 117.00 | 101.00 | 138.00 | 106.00 | 141.00 | 134.00 | 121.00 | 126.00 | 130.00 | 139.00 | 134.00 | 133.00 | 128.00 |
| W | 0.20 | 0.40 | 0.60 | 1.80 | 0.90 | 0.90 | 0.50 | 0.20 | 0.70 | 0.40 | 0.20 | 1.20 | 0.40 | 0.60 | 0.50 |
| Y | 21.60 | 9.26 | 17.78 | 12.26 | 18.32 | 10.90 | 18.16 | 20.37 | 23.16 | 24.78 | 22.63 | 22.10 | 22.24 | 21.31 | 23.26 |
| Zn | 127.00 | 18.00 | 29.00 | 93.00 | 112.00 | 14.00 | 61.00 | 97.00 | 80.00 | 102.00 | 75.00 | 110.00 | 67.00 | 69.00 | 63.00 |
| Zr | 129.50 | 149.00 | 144.30 | 199.50 | 124.10 | 136.10 | 114.20 | 114.90 | 109.60 | 102.10 | 110.60 | 118.20 | 118.90 | 142.20 | 130.40 |
| **REE** | | | | | | | | | | | | | | | |
| La | 23.80 | 25.62 | 28.72 | 41.14 | 21.39 | 23.90 | 22.67 | 22.26 | 27.12 | 26.87 | 23.31 | 23.24 | 22.33 | 22.02 | 23.44 |
| Ce | 51.31 | 55.48 | 61.32 | 83.35 | 46.20 | 51.04 | 49.25 | 48.02 | 53.34 | 56.52 | 50.62 | 50.80 | 48.40 | 47.46 | 51.06 |
| Pr | 5.94 | 6.22 | 7.01 | 9.68 | 5.29 | 6.04 | 5.59 | 5.58 | 6.39 | 6.59 | 5.78 | 5.91 | 5.55 | 5.49 | 5.87 |

| Sample | K7_47 | K7_163 | K7_84 | K7_151 | K15_393 | K15_187 | K15_280 | K15_323 | K7_202.86 | K7_203 | K11_33 | K11_65 | K15_85 | K15_131 | K15_257 |
|---|---|---|---|---|---|---|---|---|---|---|---|---|---|---|---|
| Element/ Oxyde | Rhyolite | Rhyolite | Rhyolite | Rhyolite | Rhyolite | Rhyolite | dacite | dacite | Andesite | Andesite | Andesite | Andesite | Andesite | Andesite | Andesite |
| Nd | 22.20 | 22.74 | 25.42 | 35.43 | 19.68 | 22.29 | 20.77 | 20.26 | 23.45 | 23.96 | 21.94 | 22.09 | 20.43 | 20.42 | 21.78 |
| Sm | 4.39 | 4.36 | 4.89 | 6.11 | 3.98 | 4.33 | 3.87 | 4.01 | 4.30 | 4.60 | 4.28 | 4.31 | 4.19 | 4.00 | 4.42 |
| Eu | 1.14 | 1.00 | 1.20 | 1.57 | 0.97 | 1.03 | 0.96 | 1.05 | 1.11 | 1.22 | 1.14 | 1.11 | 1.02 | 1.03 | 1.19 |
| Gd | 3.99 | 3.52 | 4.17 | 4.44 | 3.52 | 3.60 | 3.71 | 3.75 | 4.02 | 4.25 | 3.98 | 4.17 | 3.86 | 3.76 | 4.03 |
| Tb | 0.63 | 0.43 | 0.65 | 0.56 | 0.56 | 0.49 | 0.56 | 0.58 | 0.64 | 0.64 | 0.65 | 0.64 | 0.58 | 0.60 | 0.65 |
| Dy | 4.09 | 2.08 | 3.73 | 2.88 | 3.53 | 2.58 | 3.56 | 3.62 | 4.05 | 4.22 | 4.09 | 4.06 | 3.97 | 3.90 | 4.19 |
| Ho | 0.84 | 0.39 | 0.72 | 0.51 | 0.73 | 0.45 | 0.72 | 0.77 | 0.87 | 0.89 | 0.85 | 0.85 | 0.84 | 0.84 | 0.90 |
| Er | 2.49 | 1.08 | 1.97 | 1.42 | 2.21 | 1.29 | 2.16 | 2.27 | 2.52 | 2.75 | 2.53 | 2.51 | 2.51 | 2.48 | 2.64 |
| Tm | 0.39 | 0.18 | 0.29 | 0.22 | 0.35 | 0.20 | 0.33 | 0.33 | 0.39 | 0.43 | 0.39 | 0.40 | 0.39 | 0.38 | 0.39 |
| Yb | 2.29 | 1.25 | 1.83 | 1.52 | 2.19 | 1.31 | 2.05 | 2.28 | 2.56 | 2.64 | 2.47 | 2.53 | 2.35 | 2.42 | 2.48 |
| Lu | 0.35 | 0.21 | 0.26 | 0.25 | 0.34 | 0.20 | 0.31 | 0.31 | 0.38 | 0.38 | 0.35 | 0.35 | 0.32 | 0.35 | 0.36 |
| Th/Nb | 2.51 | 2.75 | 2.82 | 3.95 | 1.65 | 1.53 | 1.74 | 1.65 | 0.51 | 0.55 | 1.02 | 1.00 | 0.48 | 0.64 | 1.00 |
| Th/Yb | 2.12 | 4.09 | 3.07 | 3.85 | 1.87 | 3.30 | 2.20 | 1.95 | 1.92 | 2.05 | 1.88 | 1.95 | 1.86 | 1.80 | 1.85 |
| Th/La | 0.20 | 0.20 | 0.20 | 0.14 | 0.19 | 0.18 | 0.20 | 0.20 | 0.18 | 0.20 | 0.20 | 0.21 | 0.20 | 0.20 | 0.20 |
| Nb/Yb | 0.85 | 1.49 | 1.09 | 0.97 | 1.13 | 2.16 | 1.26 | 1.18 | 3.73 | 3.75 | 1.83 | 1.95 | 3.89 | 2.82 | 1.84 |
| La/Nb | 12.27 | 13.77 | 14.43 | 27.80 | 8.62 | 8.45 | 8.75 | 8.28 | 2.84 | 2.72 | 5.15 | 4.70 | 2.44 | 3.23 | 5.14 |
| Zr/Hf | 36.58 | 38.70 | 39.43 | 38.66 | 37.16 | 38.02 | 36.84 | 38.05 | 40.15 | 33.59 | 39.36 | 37.17 | 34.17 | 42.45 | 37.80 |
| La/Yb | 10.39 | 20.50 | 15.69 | 27.07 | 9.77 | 18.24 | 11.06 | 9.76 | 10.59 | 10.18 | 9.44 | 9.19 | 9.50 | 9.10 | 9.45 |
| *Eu/Eu | 0.83 | 0.78 | 0.81 | 0.92 | 0.79 | 0.80 | 0.77 | 0.83 | 0.81 | 0.84 | 0.84 | 0.80 | 0.77 | 0.81 | 0.86 |
| La/Yb))N | 7.07 | 13.95 | 10.68 | 18.42 | 6.65 | 12.42 | 7.53 | 6.64 | 7.21 | 6.93 | 6.42 | 6.25 | 6.47 | 6.19 | 6.43 |
| La/Sm))N | 3.40 | 3.68 | 3.68 | 4.22 | 3.37 | 3.46 | 3.67 | 3.48 | 3.95 | 3.66 | 3.41 | 3.38 | 3.34 | 3.45 | 3.32 |
| Sum_REE | 123.85 | 124.56 | 142.18 | 189.09 | 110.93 | 118.75 | 116.51 | 115.09 | 131.14 | 135.95 | 122.38 | 122.96 | 116.75 | 115.16 | 123.39 |
| Dy/Yb))N | 1.79 | 1.66 | 2.04 | 1.24 | 1.61 | 1.97 | 1.74 | 1.59 | 1.58 | 1.60 | 1.66 | 1.60 | 1.69 | 1.61 | 1.69 |
| Rb/Sr)N) | 6.67 | 24.37 | 13.83 | 4.87 | 4.44 | 8.07 | 27.14 | 12.77 | 9.85 | 7.78 | 7.30 | 10.14 | 12.10 | 7.90 | 26.43 |
| Sm/)Nd)N | 0.61 | 0.59 | 0.59 | 0.53 | 0.62 | 0.60 | 0.57 | 0.61 | 0.56 | 0.59 | 0.60 | 0.60 | 0.63 | 0.60 | 0.63 |
| Ta/La)N) | 0.22 | 0.19 | 0.17 | 0.07 | 0.25 | 0.15 | 0.26 | 0.27 | 0.46 | 0.55 | 0.38 | 0.44 | 0.48 | 0.51 | 0.35 |

Table 2: Comparison of the Mangodara volcanic rocks compositions with of the upper, middle, and lower continental crust compositions (Rudnick & Gao 2014).

| | La/Nb | Th/Nb | Th/La | Th /Yb | Nb/Yb | Zr/Hf | Nb/Ta | La/Yb |
|---|---|---|---|---|---|---|---|---|
| Upper crust | 2.58 | 0.87 | 0.33 | 5.25 | 6 | 36.7 | 13.4 | 15.4 |
| Middle crust | 2.4 | 0.65 | 0.24 | 2.95 | 4.54 | 33.9 | 16.5 | 10.7 |
| Lower crust | 1.6 | 0.24 | 0.15 | 0.8 | 3.33 | 35.8 | 8.3 | 5.3 |
| Andesite | 5.14 – 2.44 | 1.02 – 0.47 | 0.21 – 0.18 | 2.05 – 1.79 | 3.89 – 1.83 | 42.44 – 33.58 | 13.27 – 8.51 | 10.59 – 9.09 |
| Dacite | 8.75 – 8.27 | 1.74 – 1.65 | 0.20 – 0.19 | 2.20 – 1.94 | 1.26 – 1.17 | 38.04 – 36.83 | 7.91 – 7.84 | -11.05 9.76 |
| Rhyolite | -27,79 8.44 | 3.95 – 1.52 | 0.20 – 0.14 | 4.08 – 1.86 | 2.16 – 0.84 | 39.42 – 36.58 | 13.47 – 6.46 | 27.06 – 9.76 |

### *REE and multi-element data analysis*

All volcanic rocks have been normalized with rare earth element (REE) and trace element patterns of primitive mantle (McDonough & Sun 1995). In andesite, ΣREE = 105.95 to 135.95 ppm, show light rare earth elements enrichment (LREE) compared to heavy rare earth elements (HREE) and $(La/Yb)_N$ = 6.19 - 8.25, $(La/Sm)_N$ = 3.32 - 3.95 (Fig. 10a). All profiles show Eu negative anomaly with Eu/Eu* ratio = 0.72 - 0.94. The multi-element patterns of the andesite show consistent profiles with a gentle slope highlighting weak high field strength element (HFSE) (Nb, Ta, Ti), large ion lithophile elements (LILE) (Sr, Rb, Th) and P negative anomaly (Fig. 10b) and the ratios $(Rb/Sr)_N$= 4.26 – 12.09, $(Sm/Nd)_N$ = 0.56 - 0.63 and $(Nb/Th)_N$ = 0.09 - 0.25. There is also a positive Pb anomaly. Occasionally Pb shows highly positive anomaly in accordance with two samples (K7_198 and K15_257) showing strong ratio $(Rb/Sr)_N$ respectively 18.32 and 26.42. In dacite, ΣREE = 115.09 to 118.75 ppm shows concordant profiles with LREE (La à Eu) enrichment 30 to 40 times the primitive mantle compared to HREE (Gd à Lu) 3 times the primitive mantle (Fig. 10c), with $(La/Yb)_N$ = 6.64 - 12.42 and (La/Sm)N = 3.48 - 3.67, Eu/Eu* = 0.77 - 0.83. The multi-element patterns shows a gentle slope with a negative anomaly in HFSE (Nb, Ta, Ti), LILE (Sr, Th), P and positive anomaly in Pb (Fig. 10d), with $(Rb/Sr)_N$=8.07 - 27.13 and $(Sm/Nd)_N$ = 0.57 - 0.60, $(Nb/Th)_N$ = 0.06 - 0.07. The rhyolite shows variably fractionated middle REE (MREE) to HREE patterns $(Sm/Yb)_N$ = 1.97 – 4.36, enrichment in LREE compared to HREE (Fig. 10e) with $(La/Yb)_N$ = 6.65 – 18.42; in LREE compared to MREE $(La/Sm)_N$ = 3.37 – 4.22 and Eu negative anomaly (Eu/Eu* = 0.9–1.6). The rhyolite can be divided into the high and low $(Gd/Yb)_N$ groups. The trace element patterns are characterized by positive anomaly in Ba, U and Pb and negative anomaly in Sr, Nb, Ta, and Ti (Fig. 10f), with $(Rb/Sr)_N$=4.44 - 24.13, $(Sm/Nd)_N$ = 0.53 - 0.62 and $(Nb/Th)_N$ = 0.04 - 0.07.

### *Geotectonic setting*

Trace element data, particularly immobile elements, are used to discriminate tectonic settings associated with magma types (Pearce 2008, Gorton & Schandl 2000, Pearce *et al.* 1984). Using the Rb vs. Y + Nb, Nb vs. Y, Rb vs. Yb + Ta and Ta vs. Yb diagram of Pearce *et al.* (1984) volcanic rocks evolve in the same geotectonic environment (Fig. 11a-d). All volcanic formations (rhyolite, dacite, andesite) occur in the volcanic arc granite (VAG) field. In the Nb/Yb vs Th/Yb binary diagram, Pearce (2008) showed a correlation between immobile elements geochemistry and geotectonic context (Fig. 11e). Thus, the volcanic rocks of the Mangodara area lie within the volcanic arc field. According to the binary diagram Th/Yb vs. Ta/Yb, Th/Ta vs. Yb by Gorton & Schandl (2000) (Fig. 11f and g), the andesite, dacite, and rhyolite evolve in the active continental margin (ACM) with the rhyolites close to the oceanic arc and the andesites close to the intraplate volcanic zone (WPVZ).

## DISCUSSION

### Petrology

The intermediate to felsic volcanic rocks of the Mangodara sector can be divided into several types according to their petrographic and geochemical features. Although outcrops are rare and poorly preserved in the field, volcanics have been described mainly on the basis of petrographic and geophysical data as andesite, rhyolitic tuff and intermediate to felsic volcaniclastic (Metelka *et al.* 2011, Baratoux *et al.* 2011, Ilboudo *et al.* 2017, Ilboudo *et al.* 2020) and are geochemically calc-alkaline (Ilboudo *et al. 2020*).

The current study supported with drill cores examination shows a coherent and volcaniclastic tendency for meta-andesite, that is interpreted as products of explosive volcanic eruptions rich in volatile materials (Gibson *et al.* 1999, Lafrance *et al.* 2003, White *et al*. 2003, Gaboury & Pearson, 2008, Manville *et al*. 2009, Hayman *et al.* 2023). The coherent meta-andesites are particularly rich in feldspar phenocrysts and do not show a clear contact with the volcaniclastic meta-andesite. This indicates a continuum of explosive volcanism following the emplacement of feldspar phenocrysts bearing lava flows. Geochemically, they show calc-alkaline affinity, negative Eu anomaly with Eu/Eu* ratio = 0.72 - 0.94 and positive correlation between $SiO_2$ vs $(La/Sm)_N$ ratio (Fig. 12a). The negative Eu anomaly and the positive correlation between the $SiO_2$ vs $(La/Sm)_N$ ratio reflect fractional crystallization of plagioclase in the magma source. Indeed, under reducing conditions, $Eu^{3+}$ is reduced to $Eu^{2+}$ and replaces the calcium ($Ca^{2+}$) of plagioclase (Lach 2012) and the ratio of $(La/Sm)_N$ is higher due to the effect of fractional crystallization plagioclase (Mamani *et al.* 2009). These rocks also show a negative correlation between the ratio $(La/Sm)_N$ and $(Dy/Yb)_N$ (Fig. 12b) indicating therefore, fractional crystallization is dominated by amphibole in the magma source. The $(Dy/Yb)_N$ ratios are indicative of the involvement of amphiboles in themagma source (Mamani *et al.* 2009, Guo *et al.* 2020). The negative Nb, Ta, Ti and Sr anomalies and the lack of the garnet signature (i.e. a flat Dy–Yb spectrum) characterize partial melting to amphibolite facies (Mo *et al.* 2008).

Metadacite is represented only by coherent facies and corresponds to the smallest volcanic unit in the Mangodara sector. Dacitic volcanism can be interpreted as lava flows with plagioclase phenocrysts. It presents a calc-alkaline affinity with the spectra of REE and trace elements parallel

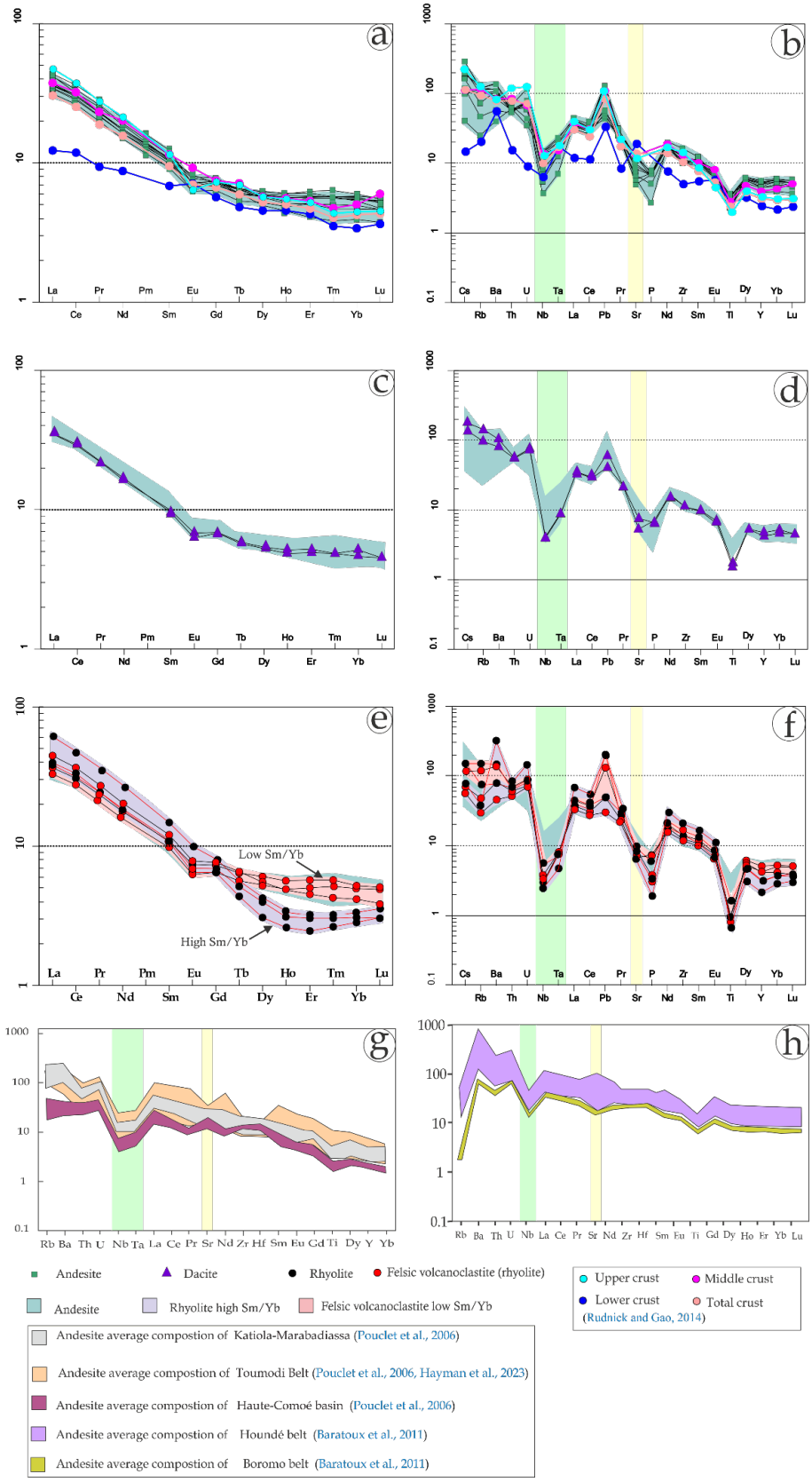


Figure 10: Primitive mantle normalized REE and spider diagram profiles (see Mc Donough, 1995) of the Mangodara volcanic rocks. (a): Primitive mantle normalized REE patterns of andesites; (b): Primitive mantle normalized spider diagram of andesite; (c): Primitive mantle normalized REE patterns of dacite; (d): Primitive mantle normalized spider diagram of dacite; (e): Primitive mantle normalized REE patterns of rhyolite; (f): Primitive mantle normalized spider diagram of rhyolite; (g): Primitive mantle normalized REE and incompatible elements diagrams (McDonough & Sun 1989) comparisons between greenstone belts of Côte d'Ivoire (modified Pouclet et al. 2006 and Hayman et al. 2023). (h) Primitive mantle normalized REE and incompatible elements diagrams (McDonough & Sun 1989) comparisons between Houndé and Boromo greenstone belts (Modified Baratoux et al. 2011).

and similar to that of andesite (Fig. 10c and d). The spectra show a negative Eu anomaly with Eu/Eu* = 0.77 - 0.83 and a positive correlation between the $SiO_2$ vs $(La/Sm)_N$ ratio (Fig. 12a) due to fractional crystallization of plagioclase in the magma source. Furthermore, the lithostratigraphic sequence established for the Banfora belts associates dacite with andesite (Baratoux *et al.* 2011, Ilboudo *et al.* 2020).

The rhyolitic units of the Mangodara sector are composed of rhyolitic tuff and volcaniclastic metarhyolite. Therefore, our data suggest that the volcanites of the sector are dominated by explosive eruption products. Texturally similar rocks have been described in the Houndé and Boromo belts (Metelka *et al.* 2011, Baratoux *et al.* 2011) and in Ivory Coast in the Toumodi, Comoé and Bandama belts (Pouclet *et al.* 2006, Mériaud *et al.* 2020, Hayman *et al*. 2023). They are interpreted as a deep-water volcanic eruption (Wite *et al.* 2003, Grenholm *et al.* 2019, Hayman *et al.* 2023). Furthermore, the metarhyolites are mainly calc-alkaline and present a negative Eu anomaly (Eu/Eu* = 0.78–0.92) indicating that the plagioclase has undergone fractional crystallization. Also, the metarhyolitic tuffs and felsic volcaniclastics present variably fractionated HREE patterns $(Dy/Yb)_N$ = 1.05 – 1.33 and an enrichment in LREE relative to the HREE $(La/Yb)_N$ = 6.65 – 18.42 in the normalized REE diagram of the primitive mantle. Thus, felsic volcanics be divided into two groups according to the enrichment in MREE relative to HREE high $(Sm/Yb)_N$ = 3.59 – 4.36 and low $(Sm/Yb_N$ = 1.97 – 2.90 (Fig. 10e and f). However, rhyolites are the result of petrogenetic processes involving partial melting, fractional crystallization and assimilation (Hart *et al.* 2004, Gaboury & Pearson, 2008). The depths at which these processes occur, magma ascent rates, and crustal residence times also influence rhyolite chemistry (Gaboury & Pearson 2008). The rhyolites of the study area compared to the classification ($Yb_N$ vs $La/Yb_N$) of Hart *et al.*(2004) define a signature FI for the rhyolite tuff and FII for the volcanic tuff (Fig. 12c). The trace element geochemistry of the different felsic magmas is determined by the residual mineral phases, in which FI magmas equilibrate with garnet residues, FII magmas equilibrate with amphibole plagioclase residues (Hart *et al.* 2004).

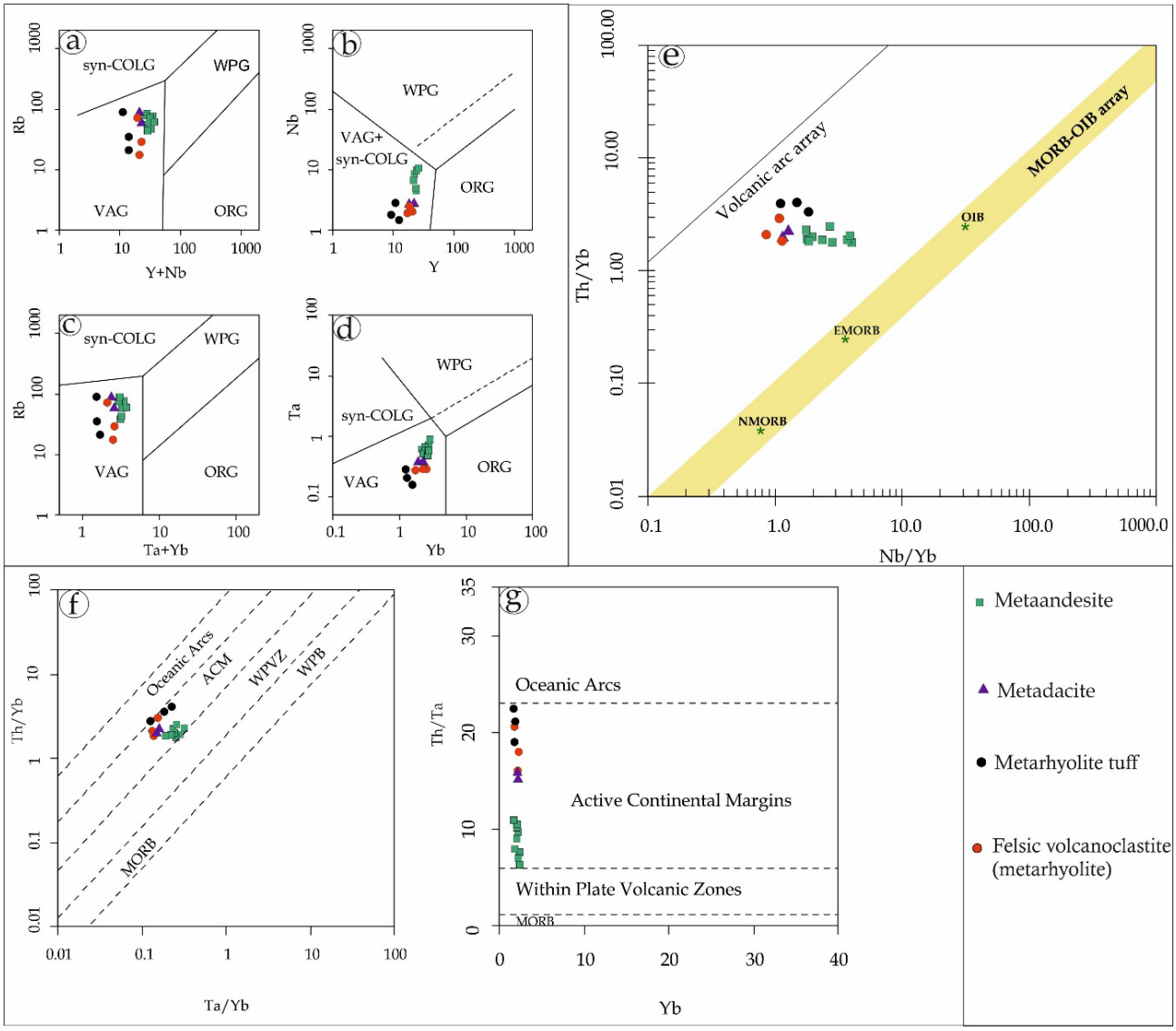


Figure 11: Geotectonic setting of the Mangodara volcanic rocks. (a - d): Diagram from Pearce et al. (1984); (e): Diagram from Pearce, 2008; (f -g): Diagram from Gorton &Schandl (2000), revised after Pearce (1983). ACM: active continental margins; WPVZ: within-plate volcanic zones; MORB: mid-ocean ridge basalts; VAG: volcanic arc granites; WPG: within-plate granites; Syn-COLG—syncollision granites; ORG—ocean ridge granites.

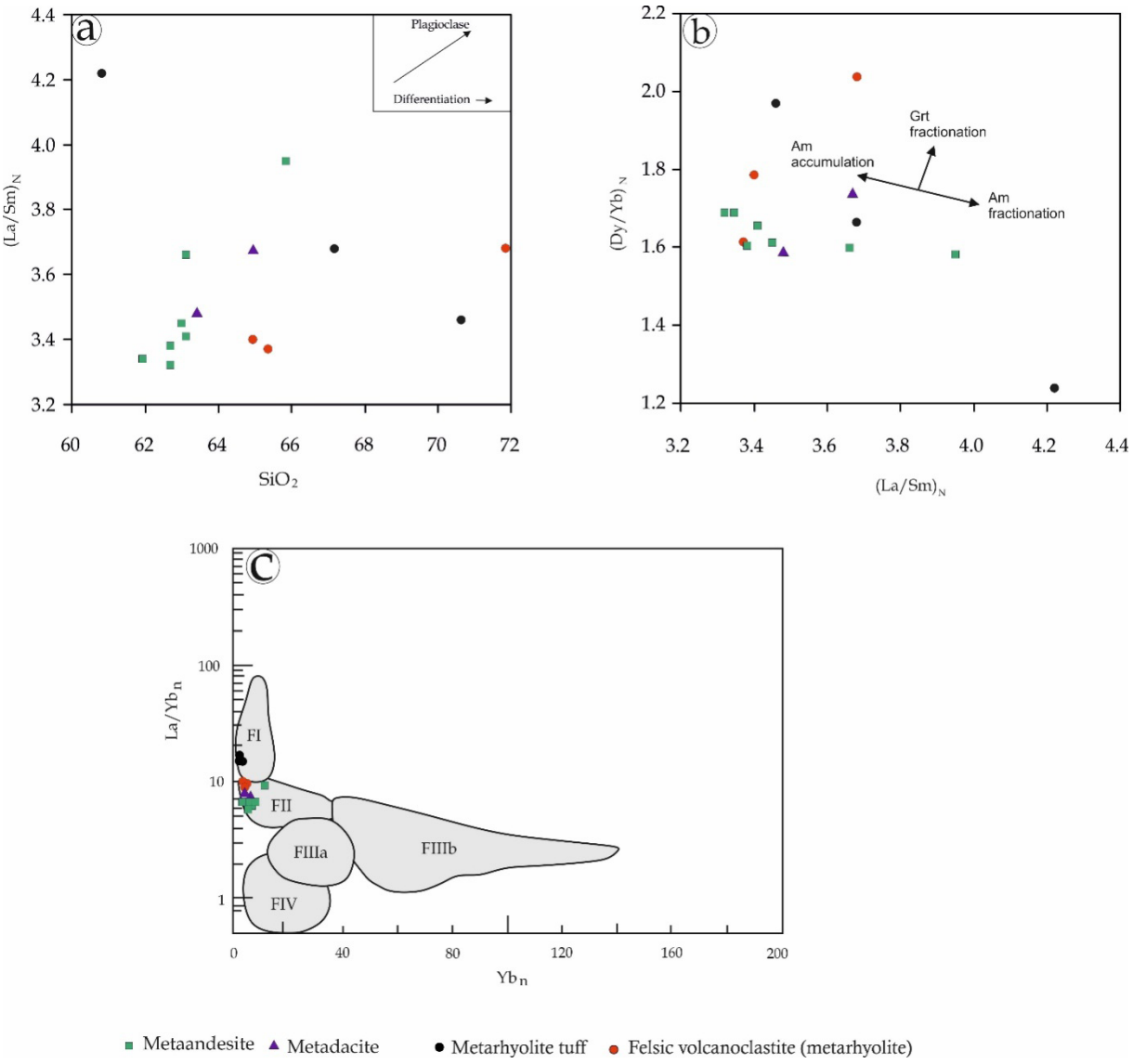


Figure 12: (a): Diagramme binaire $SiO_2$ versus $(La/Sm)_N$ ; (b): Whole-rock trace-element $(La/Sm)_N$ versus $(Gd/Yb)_N$; (d): $Yb_N$ versus $(La/Yb)_N$ (Hart *et al*. 2004).

## Potential source of lava

Incompatible trace element ratios can be used to distinguish the main crustal reservoirs. For example, Nb/Th is about 1.4 in the middle continental crust, about 15.7 in MORB and 7 in the early mantle, indicating that significant fractionation occurred during the formation of MORB and continental crust (Rollinson & Pease 2021). However, these incompatible element ratios are not affected by degrees of fractional crystallization or partial melting (Condie 1994, Münker *et al.* 2003, Pearce 2008, 2014, Boyce *et al.* 2015, Pearce *et al.* 2021). The Zr/Hf vs. Nb/Ta ratios of the rocks in the study area (andesites, dacites, rhyolites) were compared with the main reservoirs (mantle peridotites, mid-ocean ridge basalts (MORBs), ocean island basalts (OIBs), continental basalts and continental crust, Fig. 13a) to investigate their potential sources. The Mangodara volcanics are all characterized by a relatively high Zr/Hf ratio (> 30) with a relatively low Nb/Ta ratio (< 17), indicating that they originate from continental crustal sources. It is established that continental crust is depleted in Nb relative to La and has a sub-chondritic Nb/Ta ratio (<19) (Münker *et al.* 2003, Rudnick & Gao 2014). According to the La/Yb vs Th/Ta diagram (Fig. 13b), andesite lies between the Arc mantle and the upper continental crust with a higher Th/Ta ratio than MORB (> 5), while dacite and rhyolite show a higher Th/Ta ratio compared to the average upper continental crust (> 10) (Condie 1994, Rudnick & Gao 2014). This suggests that the mantle is not involved the genesis of andesitic magma at Mangodara. Multielement pattern shows negative anomalies in Nb-Ta, Sr and Ti and positive ones in Pb, as well as relatively high abundances of LILE and LREE, suggesting they may have been extracted from contaminated or metasomatized source in the middle continental crust (Hawkesworth & Kemp 2006, Parra-Avila *et al*. 2019, Picard *et al.* 1986, Rudnick & Gao 2003, 2014).

## Geodynamic setting

The geodynamic evolution of the Paleoproterozoic formations of the West African Craton is debated, but the geodynamic principles are relatively well known (Lompo 2009, 2010, Baratoux *et al.* 2011, Eglinger *et al.* 2017, Parra-Avila *et al.* 2019, Grenholm *et al.* 2019, Ilboudo *et al.* 2020, Bonzi *et al.* 2021, Ilboudo *et al.* 2021, Hayman

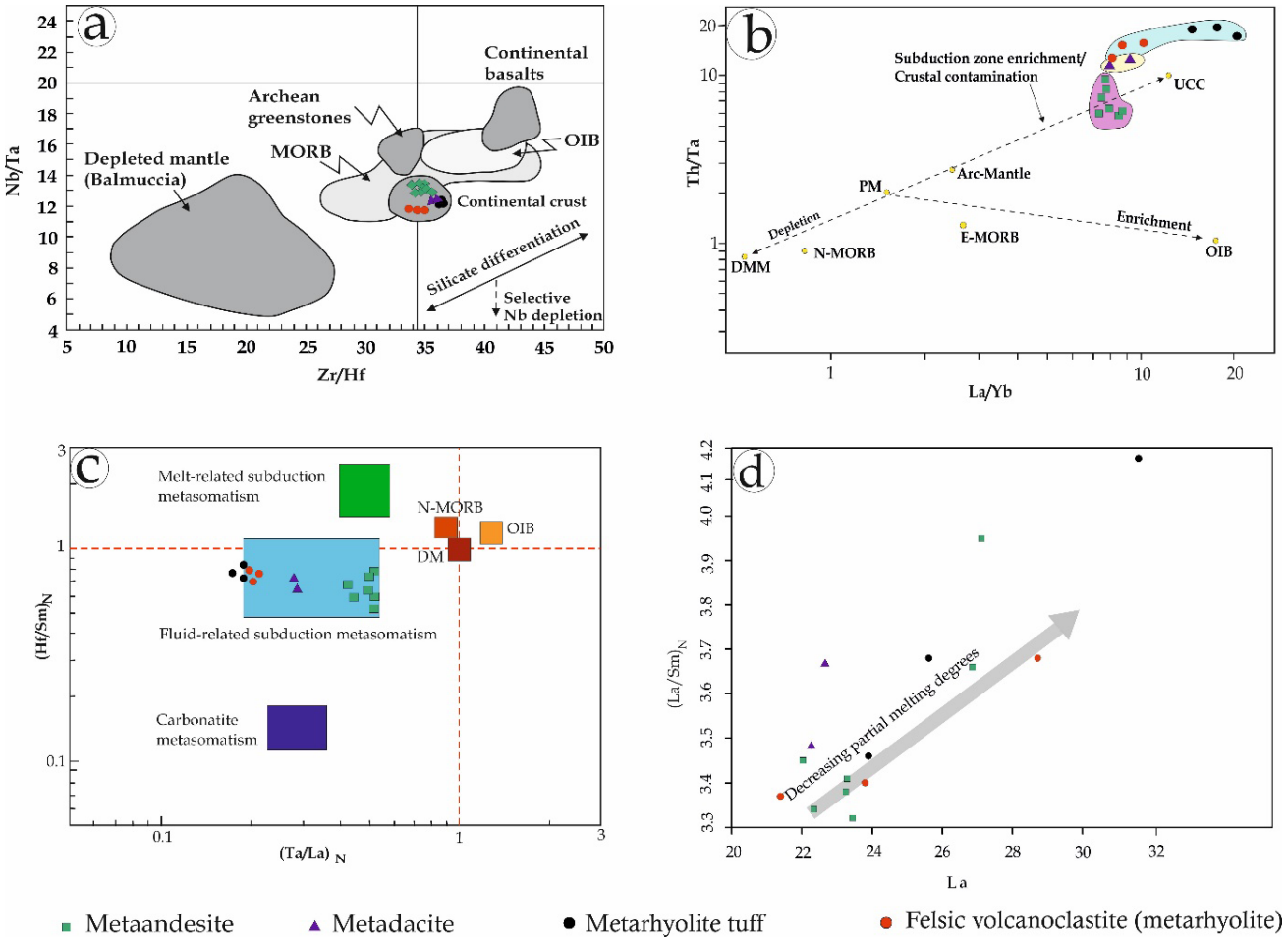


Figure 13: : (a): Plot of Nb/Ta versus Zr/Hf (Münker et al. 2003) of the Mangodara volcanic rocks ; (b) La/Yb versus Th/Ta plot (Condie 1994); (c): (Ta/La)N versus $(Hf/Sm)_N$ diagram (La Flèche *et al.* 1998) ; (d) : Whole-rock trace-element $La_N$ versus $(La/Sm)_N$ shows positive correlation.

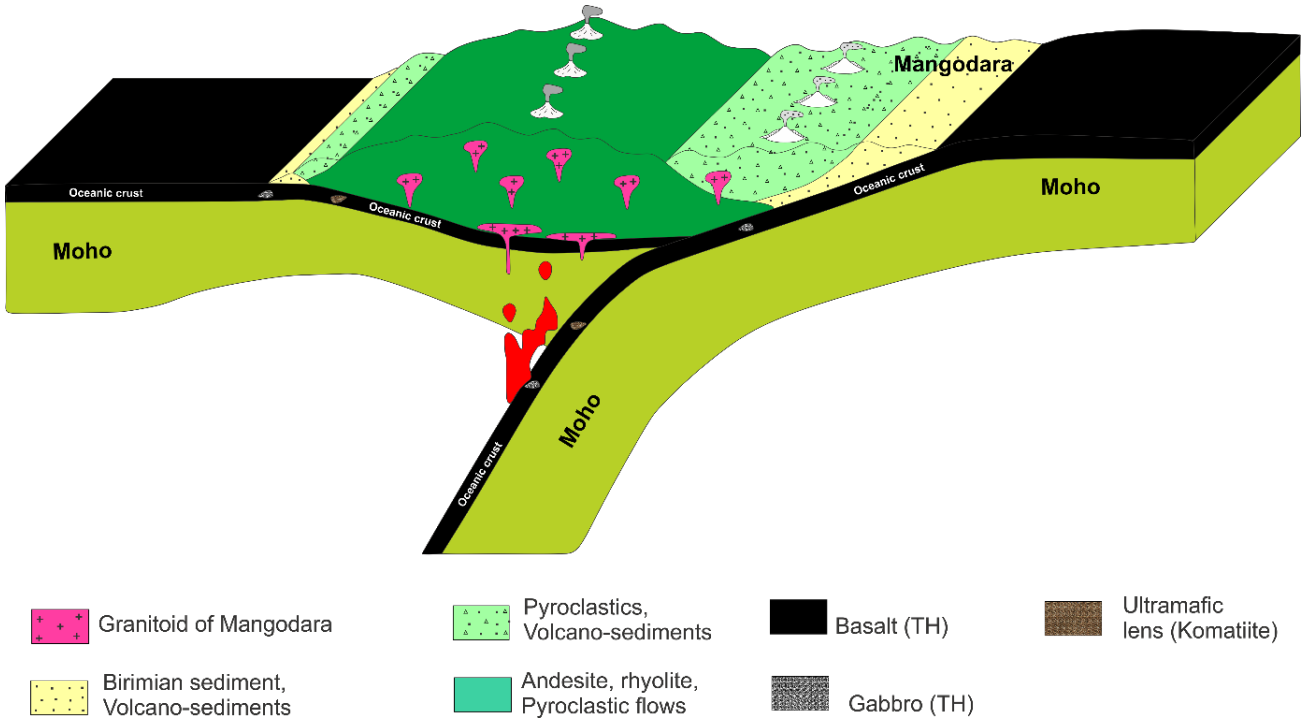


Figure 14: Geodynamic model of the Banfora belt. The surface corresponds to the current environment

*et al.* 2023). Recentworks on the Birimianbelts supports an arc-like environment (Baratoux *et al.* 2011, Petersson *et al.* 2016, Parra-Avila *et al.* 2019, Grenholm *et al.* 2019, Mériaud *et al.* 2020, Ilboudo *et al.* 2020, 2021, Hayman *et al.* 2023). Continental crust is characterized by negative Nb and Ta anomalies as well as positive Pb anomalies (Arculus *et al.* 1988, Hawkesworth & Kemp 2006, Rudnick & Gao 2003, 2014, Guo *et al.* 2020). These features, along with the low Nb/Th ratios and calc-alkaline nature of the rocks, are considered as important indicators of arc environments dominated by subduction processes (Arculus *et al.* 1988, Hawkesworth & Kemp, 2006, Hofmann, 1997, Rudnick & Gao 2003, Condie 2005, Pearce 2008, 2014, Moyen & Martin 2012, Pearce *et al.* 2021), but they can also be the result of crustal contamination and/or intracrustal melting (Mo *et al.* 2008). All volcanic rock from the study area shows strong negative anomalies in Nb, Ta, Sr and P, and a positive anomaly in Pb. We also note that, like the mid-continental crust (Fig. 10b, Rudnick et Gao, 2003, 2014), the volcanics in the Mangodara area show a negative Sr anomaly (relative to Pr and Nd), which differs from an arc magma (see Perfit *et al.* 1980, Borg *et al.* 1997, Elliott 2003, Niu & O'Hara 2003, Kelemen *et al.* 2007) that shows a positive Sr anomaly (relative to Pr and Nd). According to Mo *et al.* (2008), negative Sr anomalies (relative to Pr and Nd) are indicators of hot plate partial melting in the amphibolite stability field at depths < 40 km. This geothermal model indicates that the subduction zone is too cold, with a thermal gradient of ~ 5°C/km to melt (Mo *et al.* 2008). In the case of a cold subducted slab, it has been recognized that for the slab to melt, it must be young (< 10 Myr) (Peacock 1991). However, hydrous conditions accompanied by strong geothermal gradient caused by sustained magmatic activity, allow amphibolites to form at the expense of basalts in a subduction context (Green & Ringwood 1968). These amphibolites may then partially melt beneath the crust (at around 30 km), giving rise to the calc-alkaline series. On their ascent to the surface, these magmas undergo various fractional crystallization processes, producing the entire compositional range of calc-alkaline magmas (Green & Ringwood 1968). The negative Nb, Ta and Sr anomalies, as well as the positive Pb anomalies and low Cr and Ni content of the rocks in the study area, all point to slab melting in the amphibolite facies at the start of subduction. The environment described above could be the result of a primitive arc that did not trigger partial melting of the overlying mantle, which was too cold. On the other hand, aqueous fluids resulting from the dehydration of the subducting plate may promote partial crustal melting as they rise to the surface. As presented in the $(Ta/La)_N$ versus $(Hf/Sm)_N$ diagram (Fig. 13c), the Mangodara metavolcanites are produced by subduction-related metasomatic fluids. Furthermore, volcanic rocks show generally positive correlations in the La vs $(La/Sm)_N$ diagram (Fig. 13d), indicating that they may originate from different degrees of partial melting of the same crustal source. Therefore, the hypothetical scenario for the origin of the Banfora belt corresponds to an individual, isolated volcanic arc (Fig. 14).

**Comparison with Birimian terrains**

The geodynamic history of the Banfora belt is based on the lithostratigraphic succession presented above (Baratoux *et al*. 2011, Ilboudo *et al*. 2020). Can this evolutionary pattern be applied to all the Birimian belts in western Burkina and their continuity in Côte d'Ivoire (Fig. 1)? Because of (i) the diversity of lithologies made up of different volcanic and sedimentary rocks in distinct tectonic contexts and (ii) the controversy over the interpretation of the tectonic style that prevailed in the Birimian. The current general lithostratigraphy of the rock belts is relatively well established and supported by lithological, geochemical, structural and geochronological data. They are formed at the base by a series of metabasaltic formations (pillow basalt) of tholeiitic character with minor metasedimentary intercalations, overlain by a thick metadetritic series with carbonate intercalations associated with calc-alkaline volcanics (Lompo, 2009, Baratoux *et al.* 2011, Petersson *et al*. 2016, Augustin & Gaboury, 2017, Grenholm *et al.* 2019 , Ilboudo *et al.* 2020, Mériaud *et al.* 2020, Hayman *et al.* 2023).

However, the petrographic, geochemical and geochronological characteristics of the various greenstone belts show two main groups of lithostratigraphic successions. On the one hand, the group comprising the Banfora belt and the eastern part of the Boromo belt, presenting a basal unit of tholeiitic basalts intercalated with andesite komatiite pyroxenolite and calc-alkaline rhyolite (Baratoux *et al*. 2011, Ilboudo *et al.* 2020). On the other hand, the group representing the Houndé belt, the western part of the Boromo belt, the Toumodi belt, the Comoé belt (upper Comoé and southern Comoé), which ranges from calc-alkaline tholeiitic basalts to calc-alkaline andesite and rhyolite (Baratoux *et al*. 2011, Metelka *et al.* 2011, Petersson *et al*. 2016, Koffi *et al*. 2017, Augustin & Gaboury, 2017, 2019, Mériaud *et al*. 2020, Senyah, 2021, Nanema, 2021, Hayman *et al.* 2023). Furthermore, the mafic rocks of the Houndé belt are less evolved than those of Banfora, with a large amount of cumulative gabbros (Baratoux *et al.* 2011) so the REE and trace element spectrum of tholeiitic basalts shows no genetic link with those of Banfora (Ilboudo *et al*. 2020).

In western Burkina, calc-alkaline rhyolites are dated between 2196 ± 22 Ma and 2171 ± 7 Ma (Lompo 1991, Le Métour *et al.* 2003, Davis 1995 in Schwartz and Melcher, 2003), while absolute dating of tholeiitic basalts gives ages between 2264 ± 0.1 Ma and 2350 Ma (Nanema, 2021, Senyah, 2021). The Banfora belt is separated from the Houndé and Boromo belts by the Ouango-Fitini major shear zone, which divides the Léo Ridge into a younger western subprovince and an older eastern subprovince based on the radiometric ages of rhyolite and granite (Hirdes *et al*. 1996, Pouclet *et al.* 1996, Hirdes *et al.* 2002, Grenholm *et al.* 2019). Moreover, in Côte d'Ivoire younger ages have been found in rhyolite dated at 2170 ± 16 Ma (U - Pb) in the Toumodi belt west of the OuangoFitini shear zone (Hayman *et al*. 2023). In contrast, the Banfora belt has a εHf isotopic signature and inherited zircon ages in granites that indicate greater crustal reworking and contamination, so can be considered the boundary between these eastern and western crustal blocks of the Baoulé Mossi domain (Parra Avila *et al.* 2017, 2018, 2019). The deep-water deposits cover large areas of the Léo - Man ridge (Fig. 1) and include the Banfora, Boromo and western Houndé basins (Grenholm *et al*. 2019). They were deposited over an extended time period of 2159 +/- 4 Ma - 2097 Ma that is supported by contemporary volcanic activity (Leube *et al*. 1990, Bossière *et al.* 1996, Doumbia *et al.* 1998, Baratoux *et al*. 2011, Block *et al*. 2016, Lebrun *et al.* 2016, McFarlane, 2018, Grenholm *et al.* 2019, Hayman *et al*. 2023). The chemical composition of Banfora andesites compared with those of Houndé, Boromo, Toumodi, Comoé and Katiola-Marabadiassa show compositional differences (Fig 10b, g and h). As a result, the Mangodara andesites have a trace element composition similar to those of the Bandama, Houndé and Toumodi belts and different from that of the Comoé (see Pouclet *et al*. 2006, Baratoux *et al*. 2011, Mériaud *et al*. 2020, Senyah, 2021, Hayman *et al*. 2023). Furthermore, the Bandama and Houndé andesites show a

positive Sr anomaly, while those of Mangodara and Toumodi are characterized by negative Sr anomalies. So, the succession of tholeiitic to calc-alkaline volcanism manifests an evolution from an extensive oceanic plateau to volcanic arcs that formed between 2350 and 2160 Ma (Abouchami *et al*. 1990, Boher *et al.* 1992, Lompo, 2009, Baratoux *et al.* 2011, Augustin & Gaboury 2017, Senyah 2021, Hayman *et al.* 2023), although some authors believe that tholeiite basalts formed as oceanic ridges (Fabre 1987, Ngom *et al*. 2010, Pouclet *et al*. 2006). In addition, recent work in Côte d'Ivoire has shown that the volcanic arc formation of the Birimian system was initiated between 2200 Ma and 2160 Ma in a subaquatic environment followed by a rift at around 2160 Ma (Hayman *et al.* 2023).

## CONCLUSION

New geochemical data related to volcanism activity within the Banfora belt is provided through this present study. Volcanism appears as continuous sequence ranging from andesites to rhyolites, characterized by the combination of explosive and effusive style. (i) The andesitic volcanism of the Mangodara area is an initially explosive fluid-rich volcanism characterized by a large volume of volcanoclastic products, followed by a feldspar-phenocrystal lava. (ii) The andesite, dacite and felsic volcanoclastite show a cogenetic source, suggesting an evolution of the andesitic magma as it rises to the surface. (iii) The rhyolite REE spectrum defines a hiatus in felsic volcanism. (iv) Negative Nb, Ta, Ti and Sr anomalies and the lack of the garnet signature (i.e. a flat Dy-Yb pattern) in the andesitic magma characterize partial melting to amphibolite facies. (v) The study area describes a primitive arc that does not trigger partial melting of the overlying mantle, which is too cold, but does trigger partial melting of the middle continental crust. Volcanic rocks show generally positive correlations in the La versus $(La/Sm)_N$ diagram, indicating that they may originate from different degrees of partial melting of the same crustal source. The hypothetical scenario for the origin of the Banfora belt corresponds to an individual, isolated volcanic arc.

## ACKNOWLEDGMENT

This, work is part of the first author -Bernadin Gnamou (BG) PhD work. The author is grateful to the "Ministère de l'enseignement supérieur et de la recherche scientifique et de l'innovation" for granting three years scholarship through the Programme d'Appui à l'Enseignement Supérieur (PAES).

The authors would like to express their gratitude to the editor of «Bulletin de l'Institut Scientifique» Achab Mohammed and the journal reviewers Ilham Chraibi and Hicham Si Mhamdi for their significant contribution to the improvement of the manuscript.

## REFERENCES

Abouchami W., Boher M., Michard D.A. *et al*. 1990. A major 2.1 Ga event of mafic magmatism in West Africa : an early stage of crustal accretion. *Journal of Geophysics Research,* 95, 17605 - 17629.

Agyei Duodu J., Loh G.K., Hirdes W. *et al*. 2009. *Geological Map of Ghana 1:1000000. BGS/GGS. In: Accra*. Ghana/Hannover, Germany.

Augustin J. Gaboury D. & Crevier M. 2017. Structural and gold mineralizing evolution of the world-class orogenic Mana district, Burkina Faso: multiple mineralizing events over 150 million years. *Ore Geology Reviews,* 91, 981–1012. https://doi.org/10.1016/j.oregeorev.2017.08.007

Augustin J. & Gaboury D. 2019. Multistage and multisourced fluid and gold in the formation of orogenic gold deposits in the world-class Mana district of Burkina Faso – revealed by LA–ICP–MS analysis of pyrites and arsenopyrite. *Ore Geology Reviews,* 104, 495–522. https://doi.org/10.1016/j.oregeorev.2018.11.011

Arculus R. J., Ferguson J., Chappell B. W. *et al*.1988. Trace element and isotopic characteristics of eclogites and other xenoliths derived from the lower continental crust of southeastern Australia and southwestern Colorado Plateau USA. In *Eclogites and Eclogite-Facies Rocks (ed. D. C. Smith). Elsevier, Amsterdam*, 335–386

Arevalo R. J. & McDonough W. F. 2010. Chemical Variations and Regional Diversity Observed in MORB. *Chemical Geology,* 271, 70-85. http://dx.doi.org/10.1016/j.chemgeo.2009.12.013

Attoh, K. 1982. Structure, gravity models and stratigraphy of an early Paleoproterozoic volcanic-sedimentary belt in northeastern Ghana. *Precambrian Research,* 18, 275–290.

Babechuk M. G. & Kamber B. S. 2011. An Estimate of 1.9ga mantle depletion using the high-field-strength elements and Nd–Pb isotopes of ocean floor basalts, Flin Flon Belt, Canada. *Precambrian Research,* 189, 114-139. http://dx.doi.org/10.1016/j.precamres.2011.05.006

Baratoux, L., Metelka, V., Naba, S. *et al.* 2011. Juvenile Paleoproterozoic crust evolution during the Eburnean orogeny (~2.2–2.0 Ga), western Burkina Faso. *Precambrian Research,* 191, 18–45. http://dx.doi.org/10.1016/j.precamres.2011.08.010

Baratoux L., Metelka V., Naba S. *et al.* 2015. Tectonic evolution of the Gaoua region, Burkina Faso: Implications for mineralization. *Journal of African Earth Sciences* (Part B), 419 - 439. http://dx.doi.org/10.1016/j.jafrearsci.2015.10.004

Bassot J.P. 1987. Le complexe volcano-plutonique calco-alcalin de la rivière Daléma (Est Sénégal): discussion de sa signification géodynamique dans le cadre de l'orogénie eburnéenne (Protérozoic inférieur). *Journal of African Earth Sciences,* 6, 505 - 519.

Block S., Baratoux L., Zeh A. *et al* .2016. Paleoproterozoic juvenile crust formation and stabilisation in the south-eastern West African Craton (Ghana); New insights from U-Pb-Hf zircon data and geochemistry. *Precambrian Research,* 287, 1–30. http://dx.doi.org/10.1016/j.precamres.2016.10.011

Boher M., Abouchami W., Michard A., Albarède F., Arndt N.T., 1992. Crustal growth in West Africa at 2.1 Ga. J*ournal of Geophysics Research,* 97, 345–369.

Bonzi W., M., E., Vanderhaeghe O., Lichtervelde M., V. *et al.* 2021. Petrogenetic links between rare metal-bearing pegmatites and TTG gneisses in the West African Craton: The Mangodara district of SW Burkina Faso. *Precambrian Research,* 364, 1-38. https://doi.org/10.1016/j.precamres.2021.106359

Bonzi W., M., E., Lichtervelde M., V., Vanderhaeghe O. *et al.* 2022. Insights from mineral trace chemistry on the origin of NYF and mixed LCT + NYF pegmatites and their mineralization at Mangodara, SW Burkina Faso. *Mineralium Deposita*, 1-30. https://doi.org/10.1007/s00126-022-01127-x

Borg L. E., Clynne M. A. & Bullen T. D. 1987. The variable role of slab-derived fluids in the generation of a suite of primitive calc-alkaline lavas from the southernmost cascades, California. *The Canadian Mineralogist,* 35, 42 – 452.

Bossière G., Bonkoungou I., Peucat J.J. *et al.* 1996. Origin of Paleoproterozoic conglomerates and sandstones of the

Tarkwaian Group in Burkina Faso, West Africa. *Precambrian Research,* 80, 153 - 172

Boyce J. A., Nicholls I. A., Keays R. R. *et al.* 2015. Variation in parental magmas of Mt Rouse, a complex polymagmatic monogenetic volcano in the basaltic intraplate Newer Volcanics Province, southeast Australia. *Contributions to Mineralogy and Petrology,* 169, 1 – 21. http://dx.doi.org/10.1007/s00410-015-1106-y

Brownscombe W. 2009. *The Tinga anomaly: a new style of gold mineralisation in Ghana?* thesis, University of Oxford, MSc. 117p.

Caby R., Delor C. & Agoh O. 2000. Lithologie, structure et métamorphisme des formations birimiennes dans la région d'Odienné (Côte d'Ivoire): rôle majeur du diapirisme des plutons et des décrochements en bordure du craton de Man. *Journal of African Earth Sciences,* 30, (2), 351-374.

Castaing C., Billa M., Milési J.-P. *et al.* 2003. *Notice explicative de la carte géologique et minière du Burkina Faso à 1/1 000 000*. Bureau de Recherches Géologiques et Miniéres (BRGM), 148p.

Condie K.C. 1994. Greenstones through time, in Condie, K.C., ed., Archean crustal evolution, Chapter 3: Amsterdam, *Elsevier Scientific Publishers,* 85–120

Condie K. C. 2005. High Field Strength Element Ratios in Archean Basalts: A Window to Evolving Sources of Mantle Plumes? *Lithos,* 491-504. http://dx.doi.org/10.1016/j.lithos.2004.09.014

Condie K. C., Davaille A., Aster R. C. *et al.* 2014. Upstairs-downstairs: supercontinents and large igneous provinces, are they related? *International Geology Review,* 1 – 8. http://dx.doi.org/10.1080/00206814.2014.963170

Doumbia S., Pouclet A., Kouamelan,A. *et al.* 1998. Petrogenesis of juvenile type Birimian (Paleoproterozoic) granitoids in central Côte-d'Ivoire West Africa: geochemistry and geochronology. *Precambrian Research,* 87, 33–63. https://doi.org/10.1016/S0301-9268(97)00201-5

Eglinger A., Thébaud N., Zeh A. *et al.* 2017. New insights into the crustal growth of the Paleoproterozoic margin of the Archean Kénéma-Man domain,West African craton (Guinea): implications for gold mineral system. *Precambrian Research,* 292, 258–289. http://dx.doi.org/10.1016/j.precamres.2016.11.012

Elliott T. 2003. Tracers of the slab. *American Geophysical Union*, 23 – 45.

Fabre, R., 1987. Lithostratigraphie du Birrimien (Précambrian moyen) dans le centre de la Côte d'Ivoire (Afrique de l'Ouest), région du Yaouré. *Bulletin de la Société geologique de France*, 8, 647–663.

Feybesse J.-L. &Milesi, J.-P. 1994. The Archaean/Proterozoic contact zone in West Africa: a mountain belt of decollement thrusting and folding on a continental margin related to 2.1 Ga convergence of Archaean cratons? *Precambrian Research,* 69, 199–227.

Gaboury D. & Pearson, V., 2008. Rhyolite geochemical signatures and association with volcanogenic massive sulfide deposits: examples from the Abitibi Belt, Canada. *Economic Geology,* 103, 1531-1562.

Ganne J., Gerbault M. & Block, S. 2014. Thermo-mechanical modeling of lower crust exhumation-constraints from the metamorphic record of the Palaeoproterozoic Eburnean orogeny, West African Craton. *Precambrian Research,* 243, 88–109. http://dx.doi.org/10.1016/j.precamres.2013.12.016.

Gibson H.L., Morton R.L. & Hudak G. 1999. Submarine volcanic processes, deposits and environments favorable for the location of volcanic associated massive sulfide deposits. *Reviews in Economic Geology,* 8, 13–51.

Gorton M. &Schandl E. S. 2000. From continents to island arcs: a geochemical index of tectonic setting for arc-related and within-plate felsic to intermediate volcanic rocks. *The Canadian Mineralogist,* 38, 1065–1073. http://dx.doi.org/10.2113/gscanmin.38.5.1065

Green T.H. & Ringwood A.E, 1968. Genesis of the calc-alkaline igneous rock suite. *Contributions to Mineralogy and Petrology* 18, 105 – 162. http://dx.doi.org/10.1007/BF00371806

Grenholm M., Jessell M. & Thebaud N. 2019. Paleoproterozoic volcano-sedimentary series in the ca. 2.27–1.96 Ga Birimian Orogen of the southeastern West African Craton. *Precambrian Research,* 328, 161–192. https://doi.org/10.1016/j.precamres.2019.04.005

Guo L., Jagoutz O., Shinevar W. J. *et al.* 2020. Formation and composition of the Late Cretaceous Gangdese arc lower crust in southern Tibet. *Contributions to Mineralogy and Petrology,* 175:58. https://doi.org/10.1007/s00410-020-01696-y

Hart T. R., Gibson H. L. & Lesher C. M. 2004. Trace element geochemistry and petrogenesis of felsic volcanic rocks associated with volcanogenic massive Cu–Zn–Pb sulfide deposits. *Economic Geology,* 99, 1003–1013.

Hastie A. R., Kerr A. C, Pearce J. A. *et al.* 2007. Classification of altered volcanic island arc rocks using immobile trace elements: development of the Th-Co discrimination diagram. *Journal of Petrology,* 48, 2341-2357

Hawkesworth C., J. & Kemp A., I. S. 2006. Using hafnium and oxygen isotopes in zircons to unravel the record of crustal evolution. *Chemical Geology,* 226, 144–162.

Hayman, P.C., Bolz, P., Senyah, G. *et al.* 2023. Physical and geochemical reconstruction of a 2.35–2.1 Ga volcanic arc (Toumodi Greenstone Belt, Ivory Coast, West Africa). *Precambrian Research* 389, 1 – 19. https://doi.org/10.1016/j.precamres.2023.107029

Hein K.A.A., Matsheka I.R., Bruguier O. *et al.* 2015. The Yatela gold deposit: 2 billion years in the making. *Journal of African Earth Sciences,* 112, 548–569. https://doi.org/10.1016/j.jafrearsci.2015.07.017

Hirdes W., Davis D.W., Lu¨dtke, G. *et al.* 1996. Two generations of Birimian (Paleoproterozoic) volcanic belts in northeastern Côte d'Ivoire (West Africa), as demonstrated by precise U - Pb mineral dating: consequences for the 'Birimian controversy'. *Precambrian Research* 80, 173 - 191.

Hirdes W., & Davis DW. 2002. U-Pb geochronology of Paleoproterozoic rocks in the southern part of the Kédougou-Kénieba inlier, Senegal, West Africa: evidence for diachronous accretionary development of the Eburnean Province. *Precambrian Research*, 118, 83–99

Hirdes W, Davis DW (2002) U-Pb geochronology of Paleoproterozoic rocks in the southern part of the Kédougou-Kénieba inlier, Senegal, West Africa: evidence for diachronous accretionary development of the Eburnean Province. *Precambrian Research* 118, 83–99.

Hofmann A. W. 1997. Mantle geochemistry: The message from oceanic volcanism, *Nature,* 385, 219–229.

Ilboudo H., Wenmenga U., Sawadogo S. *et al*. 2017b. Mise en évidence d'un assemblage à disthène – staurotide – grenat dans le secteur de Mangodara, ceinture de Banfora, Burkina Faso, Afrique de l'Ouest: implication dans la genèse des gîtes minéraux polymétalliques. *Afrique Sciences,* 13, 220–231.

Ilboudo H., Sawadogo S., Zongo G. H. *et al.* 2020. Geochemistry and geodynamic constraint of volcanic and plutonic magmatism within the Banfora Belt (Burkina- Faso, West-Africa): contribution to mineral exploration. *Geological Society of London,* 502, 1–25. https://doi.org/10.1144/SP502-2019-86.

Ilboudo H., Sawadogo S., Kagambega N. *et al.* 2021. Petrology, geochemistry, and source of the emplacement model of the Paleoproterozoic Tiébélé Granite Pluton, Burkina Faso (West-Africa): contribution to mineral exploration. *International Journal of Earth Sciences,* 110, 1753–1781. https://doi.org/10.1007/s00531-021-02039-3.

Koffi Y. H., Djro S. C., Wenmenga U. 2017. Lithostructural and petrochemical Survey of Djarkadougou Gold Prospect (South West Burkina Faso / West Africa). *Earth Science Research*, 6, 155 – 174.

Kouamelan A. N. 1996. *Géochronologie et Géochimie des Formations Archéennes et Protérozoïques de la Dorsale de Man en Côte d'Ivoire. Implications pour la Transition Archéen-protérozoïque.* Thèse de Doctorat, Université de Rennes I. France (73), 289 p.

Kelemen P. B., Hanghoj K. & Greene A. R. 2007. One View of the Geochemistry of Subduction – Related Magmatic Arcs, with an Emphasis on Primitive Andesite and Lower Crust. *Treatise On Geochemistry*. *Elsevier* 3.18, 1 – 70.

Lach P. 2012. S*ignature géochimique des éléments des terres rares dans les oxydes d'uranium et minéraux associés dans les gisements d'uranium : analyse par ablation laser couplée à l'ICP-MS et étude géochronologique*. *Thèse doctorat, Université de Lorraine*, 322p

La Flèche M.R., Camiré G. & Jenner G.A. 1998. Geochemistry of post-Acadian, Carboniferous continental intraplate basalts from the Maritimes Basin, Magdalen Islands, Quebec, Canada. *Chemical Geology,* 148, 115–136.

Lafrance B., Moorhead J. & Davis D. W. 2003. *Cadre géologique du camp minier de Doyon-Bousquet-LaRonde. Géologie Québec*, *Report*, 1 - 43.

Lebrun E., Thébaud N., Miller J. et al. 2016. Geochronology and lithostratigraphy of the Siguiri district: implications for mineralisation in the Siguiri basin (Guinea, West Africa). *Precambrian Research*, 274, 136–160.

Lebrun E, Thébaud N, Miller J, Ulrich S, Bourget J, Terblanche O (2016) Geochronology and lithostratigraphy of the Siguiri district: implications for mineralisation in the Siguiri basin (Guinea, West Africa). *Precambrian Research,* 274, 136–160

Le Métour J., Chevremont P., Donzeau M. E. et al. 2003. Notice explicative de la carte géologique du Burkina Faso à 1:200 000, feuille Houndé 1-82.

Le Métour J., Chevremont P., Donzeau M. E., Thieblemont E., Tegey D., Guerrot M. C. M., Itard B., Castaing Y., Delpont C., Ki G., Zunino J. C. C. 2003. Notice explicative de la carte géologique du Burkina Faso à 1:200 000, feuille Houndé 1-82

Leube A., Hirdes W., Mauer R. *et al.* 1990. The early Proterozoic Birimian Supergroup of Ghana and some aspects of its associated gold mineralization. *PrecambrianResearch,* 46, 139 - 165.

Lompo, M. 1991. *Etude structurale et géologique des séries birimiennes de la région de Kwademen, Burkina Faso, Afrique de l'Ouest. Evolution et contrôle structural des minéralisations sulfurées et aurifères pendant l'Eburnéen*. Thèse Université de Clermont Fd, II, France, 200 p.

Lompo M., 2009. Geodynamic evolution of the 2.25-2.0 Ga Palaeoproterozoic magmatic rocks in the Man-Leo Shield of the West African Craton. A model of subsidence of an oceanic plateau. *Geological Society, London,* 323, 231–254. http://dx.doi.org/10.1144/SP323.11.

Lompo M. 2010. Paleoproterozoic structural evolution of the Man-Leo Shield (West Africa). Key structures for vertical to transcurrent tectonics. *Journal of African Earth Sciences,* 58, 19–36. http://doi.org/10.1016/j.jafrearsci.2010.01.005.

Pigois J.-P., Groves D.I., Fletcher I.R. et al. 2003. Age constraints on Tarkwaianpaleoplacer and lode-gold formation in the Tarkwa-Damang district, SW Ghana. *Mineralium Deposita*, 38, 695–714.

Pigois, J.-P., Groves, D.I., Fletcher, I.R., McNaughton, N.J., Snee, L.W., 2003. Age constraints on Tarkwaianpaleoplacer and lode-gold formation in the Tarkwa-Damang district, SW Ghana. *Mineralium Deposita*, 38, 695–714.

Mamani M., Wörner G. & Sempere T. 2010. Geochemical variations in igneous rocks of the Central Andean orocline (13°S to 18°S): Tracing crustal thickening and magma generation through time and space. *Geological Society of America Bulletin,* 122, 1-2, 162-182. http://doi.org/10.1130/B26538.1.

Manville V., Németh K. & Kano K. 2009. Source to sink: A review of three decades of progress in the understanding of volcaniclastic processes, deposits, and hazards. *Sedimentary Geology,* 220, 136–161. http://doi.org/10.1016/j.sedgeo.2009.04.022.

Markwitz V., Hein K.A.A. & Miller J. 2016. Compilation of West African mineral deposits: Spatial distribution and mineral endowment. *Precambrian Research,* 274, 61–81. http://dx.doi.org/10.1016/j.precamres.2015.05.028.

McDonough W.F. & Sun S.S. 1995. The composition of the Earth. *Chemical Geology,* 120, 223–253.

McFarlane H.B., 2018. *The geodynamic and tectonic evolution of the Paleoproterozoic Sefwi greenstone belt, West African craton*. Thèse Ph.D., Université Paul Sabatier, Toulouse, France, 265p.

Mériaud N., Thebaud N., Masurel Q. *et al.* 2020. Lithostratigraphic evolution of the Bandamian Volcanic Cycle in central Cote ˆ d'Ivoire: insights into the late Eburnean magmatic resurgence and its geodynamic implications. *Precambrian Research,* 347. https://doi.org/10.1016/j.precamres.2020.105847.

Metelka V., Baratoux L., Naba S. *et al.* 2011. A geophysically constrained litho-structural analysis of the Eburnean greenstone belts and associated granitoid domains, western Burkina Faso. *Precambrian Research,* 190, 48–69. https://doi.org/10.1016/j.precamres.2011.08.002.

Milési J.P., Feybesse J.L., Ledru P. *et al.* 1989. Les minéralisations aurifères d'Afrique de l'Ouest. Leurs relations avec l'évolution lithostructurale au Protérozoïque inférieur. *Chroniques Recherche Minière France* BRGM, 497, 3–98.

Mo X., Niu Y., Dong G. *et al.* 2008. Contribution of syncollisional felsic magmatism to continental crust growth : a case study of the Paleogene Linzizong volcanic succession in southern Tibet. *Chemical Geology,* 250, 49–67. http://dx.doi.org/10.1016/j.chemgeo.2008.02.003.

Moyen J-F. & Martin H. 2012. Forty years of TTG research. *Lithos*, 148, 312–336

Münker C., Pfänder J. A, Weyer S. *et al.* 2003. Evolution of Planetary Cores and the Earth-Moon System from Nb/Ta Systematics. *Science,* 301, 84-87. http://dx.doi.org/10.1126/science.1084662.

Nanema M. 2021. *Contraintes géologiques et facteurs de contrôle des gîtes polymétalliques de la ceinture Birimienne de Kampti, Burkina Faso - Afrique de l'Ouest*. Thèse de doctorat unique, Université Joseph KI-ZERBO, 186p.

Ngom P.M., Cordani U.G., Teixeira W. et al. 2010. Sr and Nd isotopic geochemistry of the early ultramafic-mafic rocks of the Mako bimodal volcanic belt of the Kedougou-Kéniéba inlier (Senegal). *Arabian journal of Geosciences*, 3, 49–57.

Ngom P.M., Cordani U.G., Teixeira W., Assis Janasi V., 2010. Sr and Nd isotopic geochemistry of the early ultramafic-mafic rocks of the Mako bimodal volcanic belt of the Kedougou-Kéniéba inlier (Senegal). *Arabian journal of Geosciences,* 3, 49–57.

Niu Y. & O'Hara M. J. 2003. Origin of ocean island basalts: A new perspective from petrology, geochemistry, and mineral physics considerations. *Journal of geophysical research,* 108, 1 – 19. http://dx.doi.org/10.1029/2002JB002048.

Niu Y. & O'Hara M. J. 2009. MORB mantle hosts the missing Eu (Sr, Nb, Ta and Ti) in the continental crust: New perspectives on crustal growth, crust – mantle differentiation and chemical structure of oceanic upper mantle. *Lithos,* 112, 1 – 17. http://dx.doi.org/10.1016/j.lithos. 2008.12.009.

Ouattara G. 1998. *Structure du Batholite de Ferkessédougou (Secteur de Zuenoula, Côte d'Ivoire*). Thèse Doctorat de l'Université d'Orléans, 291p.

Ouiya P., Siebenaller L., Salvi S. *et al.* 2016. The Nassara Gold Prospect, Gaoua District, Southwestern Burkina Faso. *Ore Geology Reviews,* 78, 623-630. https://doi.org/10.1016/j.oregeorev.2015.11.026.

Ouiya P., Naba S., Ilboudo H. *et al.* 2020. Mise en évidence de structures principales et connexes contrôlant la minéralisation dans le district aurifère de Nassara au sud-ouest du Burkina Faso (Afrique de l'ouest). *Journal des sciences* 20, 1-21.

Ouiya P., Yaméogo A. O., Ilboudo H. *et al.* 2022. Implication de la fertilité des basaltes paléoprotérozoïques lié à l'activité Mantle Plume à Nassara Minéralisation aurifère (Burkina Faso, Ouest Afrique). *Open Journal of Geology,* 12, 1013-1031. https://doi.org/10.4236/ojg.2022.1211048.

Palme H., & O'Neill H. 2014. Cosmochemical estimates of mantle composition. *In: Holland, H.D., Turekian, K.K. (eds.), Treatise on geochemistry, 2nd ed. Elsevier, Oxford*. 3: 1–39. http://dx.doi.org/10.1016/B978-0-08-095975-7.00201-1.

Palme H. & O'Neill H., 2014. *Cosmochemical estimates of mantle composition.* In: Holland, H.D., Turekian, K.K. (eds.), Treatise on geochemistry, 2nd ed. Elsevier, Oxford. 3: 1–39. http://dx.doi.org/10.1016/B978-0-08-095975-7.00201-1

Parra-Avila L.A., Kemp A.I.S., Fiorentini M.L. *et al.* 2017. The geochronological evolution of the Paleoproterozoic Baoulé-Mossi domain of the Southern West African Craton. *Precambrian Research,* 300, 1–27. http://dx.doi.org/10.1016/j.precamres.2017.07.036.

Parra-Avila L.A., Belousova E., Fiorentini M.L. *et al.* 2018. Zircon Hf and O-isotope constraints on the evolution of the Paleoproterozoic Baoulé- Mossi domain of the southern West African Craton. *Precambrian Research,* 306, 174–188. https://doi.org/10.1016/j.precamres.2017.12.044.

Parra-Avila L.A., Baratoux L., Eglinger A. *et al*. 2019. The Eburnean magmatic evolution across the Baoule-Mossi domain: geodynamic implications for the West African Craton. *Precambrian Research,* 332, 1 – 20. https://doi.org/10.1016/j.precamres.2019.105392.

Peacock S.M. 1991. Numerical Simulation of Subduction Zone Pressure-Temperature Time Paths: Constraints on Fluid Production and Arc Magmatism. *Philosophical Transactions of the Royal Society, A* 335, 341 – 353. https://doi.org/10.1098/rsta.1991.0050.

Pearce J.A. 1983. Role of subcontinental lithosphere in magma genesis at active continental margins. In : C.J. Hawkesworth & J. Norry, Eds., Continental basalts and mantle xenoliths. *Shiva Geology Series, Nantwich,* 230-249.

Pearce J.A., Harris N.B.W. &Tindle, A.G. 1984. Trace element discrimination diagrams for the tectonic interpretation of granitic rocks. *Journal of Petrology,* 25, 956–983.

Pearce J. A. 1996. A user's guide to basalt discrimination diagrams. *Geological Association of Canada Special Publication,* 12, 79-113.

Pearce J. A. 2008. Geochemical Fingerprinting of Oceanic Basalts with Applications to Ophiolite Classification and the Search for Archean Oceanic Crust. *Lithos,* 100, 14-48. http://dx.doi.org/10.1016/j.lithos.2007.06.016.

Pearce J.A. 2014. Immobile element fingerprinting of ophiolites. *Elements,* 10, 101–108 http://dx.doi.org/10.2113/gselements.10.2.101.

Pearce J.A., Ernst R.E., Peate D.W. *et al.* 2021. LIP printing: Use of immobile element proxies to characterize Large Igneous Provinces in geologic record. *Lithos*, 106068, 392 - 393. https://doi.org/10.1016/j.lithos.2021.106068.

Perfit M. R., Brueckner H., Lawrence J.R. *et al.*1980. Trace element and isotopic variations in a zoned pluton and associated volcanic rocks, Unalaska Island, Alaska: a model for fractionation in the Aleutian calc-alkaline suite. *Contributions to Mineralogy and Petrology,* 73, 69-87.

Petersson A., Scherstén A., Kemp A. I. S. *et al.* 2016. Zircon U–Pb–Hf evidence for subduction related crustal growth and reworking of Archaean crust within the PalaeoproterozoicBirimian terrane, West African Craton, SE Ghana. *Precambrian Research,* 275, 286–309. http://dx.doi.org/10.1016/j.precamres.2016.01.006.

Picard C. &Piboule M. 1986. Pétrologie des roches volcaniques du sillon de roches vertes archeennes de Matagami - Chibougamau l'ouest de Chapais (Abitibi est, Québec). 1. Le groupe basal de Roy. *Canadian Journal of Earth Sciences,* 3, 561 – 578.

Pouclet A., Vidal M., Delor C. *et al.* 1996. Le volcanisme birimien du nord-est la Côte d'Ivoire, mise en évidence de deux phases volcano-tectoniques distinctes dans l'évolution géodynamique du Paléoprotérozoïque. *Bulletin de la Société géologique de France,* 167, 529-541.

Pouclet A., Doumbia S. & Vidal M., 2006. Geodynamic setting of the Birimian volcanism in central Ivory Coast (western Africa) and its place in the Palaeoproterozoic evolution of the Man Shield. *Bulletin de la Société géologique de France,* 177, 105–121.

Rollinson, H., 2016. Archaean crustal evolution in West Africa: A new synthesis of the Archaean geology in Sierra Leone, Liberia, Guinea and Ivory Coast. *Precambrian Research,* 281, 1–12. http://dx.doi.org/10.1016/j.precamres.2016.05.005

Rollinson H., R. & Pease V. 2021. *Using geochemical data: to understand geological processes.* Second edition; Cambridge University Press, 1-662. http://doi:10.1017/9781108777834.

Rudnick R.L., & Gao S. 2003. Composition of the Continental Crust. In: Turekian, H.D.H.K. (Ed.). *Treatise on Geochemistry*. Pergamon, Oxford 3, 1–64.

Rudnick R. L. & Gao S. 2014. Composition of the continental crust. In: Holland H, Turekian K (eds) Treatise on geochemistry, 2nd edn. Elsevier, Oxford, 3, 1–51. http://dx.doi.org/10.1016/B978-0-08-095975-7.00301-6

Schwartz MO, Melcher F. 2003. The Perkoa zinc deposit, Burkina Faso. *Economie Geology, 98*, 1463–1485

Senyah G. A. 2021. *Volcanic architecture of the Houndé and Boromo greenstone belts, west-Africa : Implication for terrane evolution*. Doctor of Philosophy, Queensland University of Technology, 241p

Sylvester P.J. & Attoh K. 1992. Lithostratigraphy and Composition of 2.1 Ga Greenstone Belts of the West African Craton and Their Bearing on Crustal Evolution and the Archean-Proterozoic Boundary. *Journal of Geology,* 100, 377–393.

Vidal M., Gumiaux C., Cagnard F. *et al.* 2009. Evolution of a Paleoproterozoic "weak type" orogeny in the West African Craton (Ivory Coast). *Tectonophysics,* 477, 145–159. http://dx.doi.org/10.1016/j.tecto.2009.02.010.

Winchester J.A. & Floyd P.A. 1977. Geochemical discrimination of different magma series and their differentiation products using immobile elements. *Chemical Geology,* 20, 325–343. https://doi.org/10.1016/0009-2541(77)90057-2.

White J. D. L., Smellie J. L. & Clague D. A., 2003. Introduction: A Deductive Outline and Topical Overview of Subaqueous Explosive Volcanism. *American Geophysical Union,* 1 – 23.

Manuscrit reçu le 11/07/2023
Version révisée acceptée le 07/05/2024
Version finale reçue le 13/05/2024
Mise en ligne le 04/06/2024